Quaternary Science Reviews 378 (2026) 109852

Contents lists available at ScienceDirect

Quaternary Science Reviews

journal homepage: www.elsevier.com/locate/quascirev

Rapid deglacial retreat of a regional scale ice stream and late Holocene readvance in Vincennes Bay, east Antarctica

Marcello G. Blaxell [a,*], David Small [b], David Fink [c], Réka-H. Fülöp [c], Alexandru T. Codilean [d], Alexandra Post [e], Klaus Wilcken [c], Toshiyuki Fujioka [f], Sonja Berg [g], Ian Goodwin [h,i], Steven Phipps [j], Matthew R. Jeromson [a,k], Duanne A. White [a,k]

[a] Centre for Applied Water Science, Institute for Applied Ecology, University of Canberra, ACT, Australia, 2601
[b] Department of Geography, Durham University, Durham, DH1 3LE, United Kingdom
[c] Australian Nuclear Science and Technology Organisation (ANSTO), Lucas Heights, NSW, 2234, Australia
[d] School of Science, University of Wollongong, Wollongong, NSW, 2522, Australia
[e] Geoscience Australia, ACT, 2609, Australia
[f] Centro Nacional de Investigación sobre la Evolución Humana (CENIEH), Burgos, Spain
[g] Institute of Geology and Mineralogy, University of Cologne, 50674, Cologne, Germany
[h] ARC Australian Centre for Excellence in Antarctic Science, Climate Change Research Centre, University of New South Wales, NSW, 2052, Australia
[i] School of Natural Sciences, Macquarie University, NSW, 2113, Australia
[j] Ikigai Research, Hobart, TAS, 7006, Australia
[k] ARC Australian Centre for Excellence in Antarctic Science, University of Canberra, Canberra, Australia

A R T I C L E I N F O

Keywords:
Interglacial
Holocene
Glaciology
Cosmogenic isotopes
Geomorphology
Glacial
East Antarctica
Retreat timing
Readvance
Vincennes bay

A B S T R A C T

Vincennes Bay provides a unique opportunity to understand the role of bed topography on modulating deglaciation in East Antarctica. Here, one of the deepest troughs on the margin (Vanderford Trough), lies adjacent to a terrestrially grounded, independent ice dome (Law Dome). Thus, we contrast the deglacial history of these systems and provide insights into future ice loss in parts of the continent underlain by large subglacial basins.

We use multibeam bathymetry to map the ice retreat of these systems and cosmogenic nuclide dating onshore, to constrain timing. Bedforms suggest at least two phases of retreat across the continental shelf, separated by a large mid-shelf ridge. Seaward of the ridge, bedforms evidence ice sheet expansion to the continental shelf break. Landward of the ridge distinct bedforms, combined with synchronous exposure of the Windmill Islands and Snyder Rocks ~10 ka, are consistent with a Marine Ice Sheet Instability style retreat into the overdeepened troughs.

This timing evidences a distinct difference in deglacial histories in East Antarctica, with regions east of 60°E stabilising several thousand years earlier than to the west. We explore drivers of this divergence, including the potential for continental shelf geometry to limit warm water incursion to overdeepened grounding lines.

Lastly, a gap in exposure age distribution and the reworking of marine material into modern day shear moraines suggest the western margin of Law Dome was retreated further than present ~5.7 to 2.3 ka, with readvance potentially driven by a strengthening of easterly winds after ~4 ka.

1. Introduction

The East Antarctic Ice Sheet (EAIS) is the world's largest mass of land-based ice, holding ~52 m of equivalent sea level (Morlighem et al., 2020; Pritchard et al., 2025). Large swathes of the EAIS from Wilhelm II Land to George V Land, are grounded below sea level, with inland-facing slopes that are potentially prone to rapid retreat during times of rising sea levels and/or higher ocean temperatures, similar to those of the West Antarctic Ice Sheet (WAIS) and Greenland Ice Sheet (GrIS) (Fretwell et al., 2013; Morlighem et al., 2020; Stokes et al., 2022).

Over the past two decades satellite observations show a dramatic increase in ice-flow velocities and ice thinning of major outlet glaciers of

* Corresponding author
E-mail address: marcello.blaxell@canberra.edu.au (M.G. Blaxell).

https://doi.org/10.1016/j.quascirev.2026.109852
Received 7 October 2025; Received in revised form 29 January 2026; Accepted 1 February 2026
Available online 17 February 2026

these portions of the EAIS, however the changes are recent and may not have had time to proliferate up stream (Flament and Rémy, 2012; Helm et al., 2014; Pritchard et al., 2009). There has also been a decline in the ice shelf thickness, at rates similar to those in the WAIS (Davison et al., 2023). Ice shelves are critical for slowing the rate of ice discharge from glaciers, through buttressing (Dupont and Alley, 2005; Gudmundsson, 2013) and their loss is linked to the acceleration and thinning of ice streams; a prime example being the rapid collapse of Larsen A and B ice shelves in Antarctic Peninsula in the mid to late 1990's and early 2000's (Rignot et al., 2004; Rott et al., 1996; Scambos et al., 2004). Furthermore, there has been a significant decline in Southern Hemisphere sea ice since 2016 (Eayrs et al., 2021), with 2023 the lowest summer minimum on record, with 36% less ice area than the 1979–2022 average daily minimum (Purich and Doddridge, 2023; Schroeter et al., 2023). A similar drop in sea ice coverage was recently linked to high CO_2 levels and the onset of deglaciation post Last Glacial Maximum (LGM) (Sadatzki et al., 2023). Despite the mounting evidence of ice loss from the EAIS, there is still considerable debate on the climate states needed to trigger rapid deglaciation as well as the potential timing and magnitude of future ice loss. Projected response times range from centuries to millennia, with model estimates of the contribution to sea level varying considerably; from ~0.3 to 3 m over the next century (DeConto et al., 2021; Edwards et al., 2021; Golledge et al., 2015; Pollard and Deconto, 2016; Schlegel et al., 2018). These models use past ice sheet behaviour as calibration for future predictions and a primary cause of modal variability has been attributed to large portions of the EAIS having few constraints on deglaciation magnitude and timing (Mackintosh et al., 2011; Stokes et al., 2022).

This paper focusses on one such region, Vincennes Bay, a key section of the EAIS that is grounded largely below sea level and is susceptible to both atmospheric and ocean warming. Significantly, this makes the region at heightened risk of retreat or collapse compared to sectors of the EAIS that are grounded largely above sea level (Pelle et al., 2020). The region drains ~0.67 m of global sea level equivalent ice (Morlighem et al., 2020) and can therefore make significant contributions to sea level rise, with modern measurements suggesting that this is already occurring (e.g. McCormack et al., 2023; Picton et al., 2023). To better understand and model the future ice dynamics of the region in a warming climate, an improved understanding of past dynamics is required, such as through the addition of geological constraints on deglacial timing in Vincennes Bay. Furthermore, Vincennes Bay is uniquely positioned adjacent to Law Dome, a ~200 km wide ice dome which is largely grounded above sea level, or in shallow water, pinned to various topographic highs that sit above sea level. This allows for us to contrast glacial dynamics between these two systems, that are rarely seen in such proximity.

1.1. Aims

This work aims to provide improved constraints on ice dynamics and ice sheet retreat patterns particularly in the period since the LGM. Of particular interest are the main phase of deglaciation post LGM and the smaller fluctuations in the ice margin that may have occurred through the Holocene (Goodwin, 1996; Goodwin et al., 2018). To that end, we present a new interpretation of off-shore multibeam bathymetric data, a series of new ^{10}Be exposure ages from glacial erratics, ^{14}C ages from marine sediments embedded in a supraglacial moraine, and weathering and erosion characteristics of the sampled locations.

We combine our new data with prior work to investigate two main ideas.

1. That the timing of deglaciation post LGM reflects enhanced sensitivity of glacial basins grounded largely below sea level to a warming climate through enhanced ocean forcing.
2. That changes to atmospheric circulation could have been a key driver of changes in ice extents of both marine and terrestrially grounded ice.

1.2. Regional setting

The section of the EAIS that drains into Vincennes Bay sits within the Aurora sub-glacial basin. The Aurora basin is largely below sea level (Fig. 1) (Fretwell et al., 2013; Morlighem et al., 2020; Pritchard et al., 2025) and the ice sheet in this area is therefore likely sensitive to a warming climate, as seen in geographically similar regions during the warmer parts of the Pliocene and Pleistocene (Blackburn et al., 2020; Cook et al., 2013; Pollard and Deconto, 2016; Wilson et al., 2018). The largest ice stream that drains into the bay is the Vanderford Glacier, a fast-flowing marine based system which enters from the southeast. To the west several smaller ice streams also enter the bay, including the Adams and Underwood Glaciers. The eastern flank of Vanderford Glacier abuts Law Dome, a largely terrestrially grounded, slow-flowing ice rise.

1.2.1. Vanderford Glacier

In recent decades the Vanderford Glacier has shown signs of increasing ice mass loss, with consistent ice-surface lowering between 2003 and 2017, increasing in rate between 2017 and 2020, a signal also picked up in observations from the neighbouring Underwood, Adams and Anzac Glaciers (Picton et al., 2023). The modern grounding line is currently retreating at a rate of 0.8 km/yr, one of the highest in the EAIS, which is comparable to observations from the WAIS and suggestive of basal melt or bed geometry as driving factors of retreat (Picton et al., 2023; Stokes et al., 2022). Although the grounding line is currently on a prograde bed (Rignot et al., 2019), the majority of Vanderford Trench upstream of the grounding line sits on the reverse slope of a deep subglacial trough, falling to over 2500 m below sea level (McCormack et al., 2023), making it susceptible to Marine Ice Sheet Instability (MISI) (Jones et al., 2015; Schoof, 2007). Recent studies have also shown that ice shelves within the Vincennes Bay region lost 34% of their mass between 1997 and 2021 (Davison et al., 2023), supporting the idea that oceanic conditions are a prominent driver of ice mass loss in this system.

1.2.2. Law **Dome**

To the east of Vincennes Bay lies Law Dome (Fig. 1), a coastal ice accumulation zone formed through cyclonic activity over the Southern Ocean (Bromwich, 1988; Udy et al., 2021), providing an important link to lower latitude palaeo-climate (Udy et al., 2022; Vance et al., 2013). Law Dome has remained an independent ice mass (Pfitzner, 1980), although it is surrounded to the south-east and -west by the Vanderford and the Totten glacier systems. Several ice cores have been sampled from near the Law Dome summit and on its flanks, providing local records of palaeo-atmosphere and snow accumulation, proximal to our study region (e.g. Jong et al., 2022; Morgan et al., 1997).

Vanderford Glacier and Law Dome both have ice-free areas near the grounding line, which extend through the Windmill Islands and offshore, making them ideal locations to study past ice extents and the timings of ice retreats through the Holocene (e.g. Carson et al., 2017; Emslie and Woehler, 2005; Goodwin, 1993a, 1993b, 1996; Kirkup et al., 2002).

1.2.3. Windmill Islands

The Windmill Islands are a series of ice-free islands and outcrops that provide considerable evidence for previous glaciation in the region (Fig. 2). The northern Windmill Islands are underlain by Mesoproterozoic granulite-facies bedrock with Charnockite prevalent throughout the southern portion, including Browning Peninsula (Blight and Oliver, 1977; Paul et al., 1995; Zhang et al., 2012). The geology of northern Windmill Islands is generally less weathered and more low-lying compared to the Charnockite in the south. This 'fresher' rock better

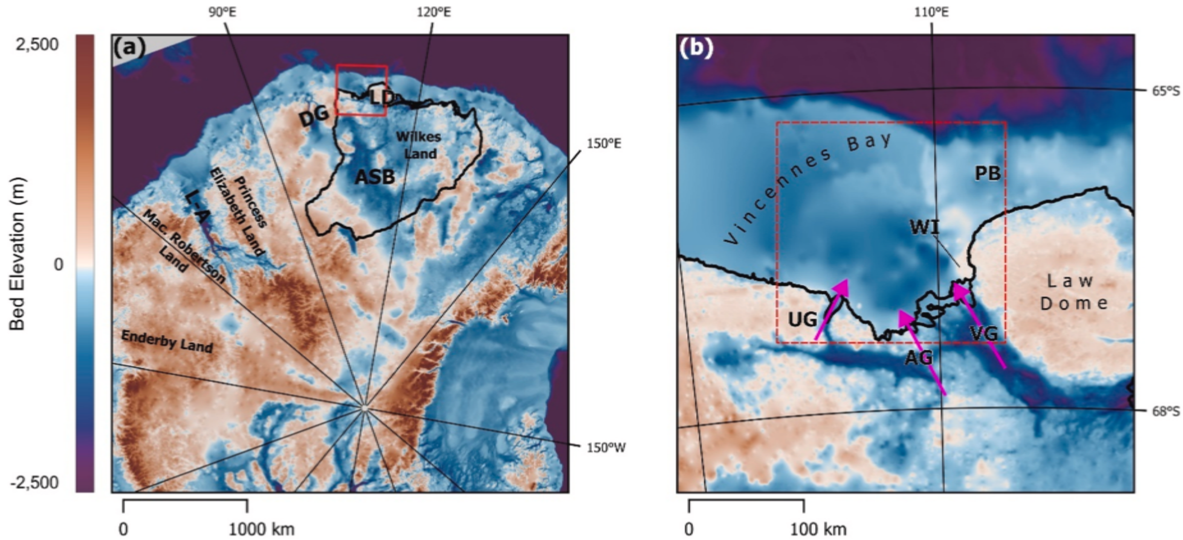

Fig. 1. Regional setting of Vincennes Bay. Panel (**a**) shows East Antarctic bed elevation (m) based on the Bedmap3 dataset (Pritchard et al., 2024). ASB outline created from GSFC 'Ice Boundaries' dataset (Zwally et al., 2012). The red inset is shown in panel (**b**). Panel (**b**) provides greater local geographic context. The dashed red inset is the location of Fig. 2, where this study is focussed. Data are referenced to the WGS 84. Panel (**a**) and (**b**) locations are Lambert Amery (**L-A**), Denman Glacier (**DG**), Aurora Subglacial Basin (**ASB**), Underwood Glacier (**UG**), Vanderford Glacier (**VG**), Windmill Islands (**WI**), Adams Glacier (**AG**) and Petersen Bank (**PB**). **Magenta** arrows represent flow direction of ice streams. (For interpretation of the references to colour in this figure legend, the reader is referred to the Web version of this article.)

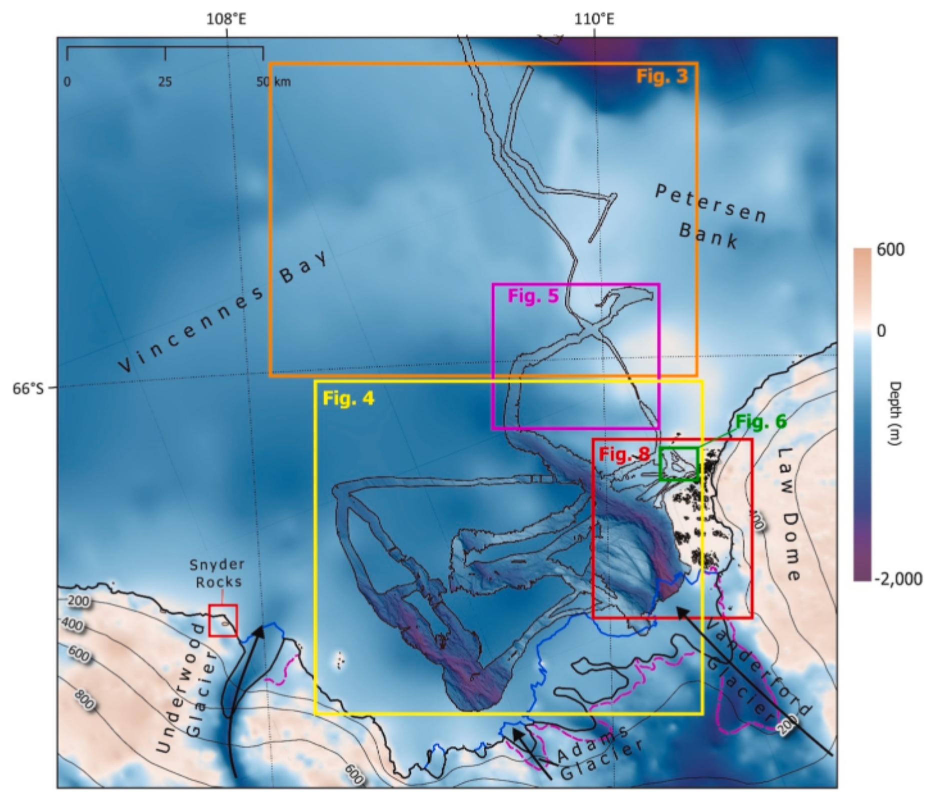

Fig. 2. Overview of Terrestrial sample locations, bathymetric and multibeam data. The base layer includes the Bedmap3 dataset (Pritchard et al., 2024) integrated with IBSCOv2 bathymetry data offshore (Dorschel et al., 2022). The bathymetric image highlighted with a black outline is the multibeam from the 2021–2022 and 2023–2024 ANARE Antarctic seasons [dataset] (Commonwealth of Australia, 2022, 2024) referenced to WGS 84. Coloured rectangles represent the extents of the maps used for bathymetric interpretations in the results (section 3.1). Fig. 3 **(orange):** Outer continental shelf. Fig. 4 **(yellow):** Inner Continental shelf. Fig. 5 (magenta): Petersen Bank. Fig. 6 (green): Law Dome Shallows. Fig. 8 (red): Ice-free areas sampled for exposure ages and weathering observations. **Black** arrows represent flow direction of modern ice streams and the. The **blue outline** is the ice shelf and the **black** is the grounding line as of 2009, taken from the MEaSUREs Antarctic boundaries dataset (Mouginot et al., 2017). The dashed magenta line is the grounding line as of 2020 as per the Antarctic Ice Sheet Climate Change Initiative (AIS CCI) dataset (Picton et al., 2023). (For interpretation of the references to colour in this figure legend, the reader is referred to the Web version of this article.)

preserves the glacial polish, chatter marks and striae found throughout the region, with a greater amount of unconsolidated glacial sediments present. Evidence such as raised beaches with elevations of up to ~30m have been mapped around the Windmill Islands (Goodwin, 1993a) indicating local sea level was ~30 m higher post LGM deglaciation with the decrease to current levels being due to isostatic rebound (Whitehouse et al., 2012). The islands are scattered with an abundance of glacial debris and sediments, evidencing the ice histories of the various ice drainages in the Aurora sub-glacial basin (Goodwin, 1993a).

Recent high resolution bathymetric studies evidence a prior expansion of Law Dome onto the continental shelf. The pattern of ice expansion from Law Dome is largely controlled by the underlying SE–NW and E–W fault systems and valleys/troughs created from multiple cycles of advance and retreat. Imposed on these older features, is more recent evidence of 'stepped' ice retreat (Carson et al., 2017). Whilst post-dating the LGM, the precise timing of this retreat is not yet clear due to lack of geochronological dating of glacial features in the region.

2. Methods

This study is designed to improve upon our understanding of deglacial patterns and timing of the EAIS in Vincennes Bay, post-LGM. We utilise recent high resolution bathymetric datasets (Commonwealth of Australia, 2022, 2024) to interpret glacial landforms on the continental shelf and observations of weathering and erosion onshore to build a relative chronology of the ice sheet retreat. We then use ^{10}Be exposure dating of glacial erratics and ^{14}C dating of marine fragments entrapped in a moraine sequence to constrain the timing of when the EAIS reached near modern extents, and whether there have been further changes in regional ice extent through the Holocene.

2.1. Bathymetry

Where available we use Multibeam bathymetry data from the 2021–2022 and 2023–2024 ANARE Antarctic seasons [dataset] (Commonwealth of Australia, 2022, 2024) of the Vincennes Bay seafloor (Fig. 2). Features were mapped manually using ArcGIS and QGIS, to create digital representations of glacial landforms including lineations, moraines, iceberg scours, grounding zone wedges (GZW) and smoothed bedrock features. As the dataset has variable resolution, features were mapped at a macro (>1 km) and meso (1m-1 km) scale and topographic profiles were measured using QGIS. Landform definitions are based on Bennett and Glasser (2009) and Carson et al. (2017). To supplement these data we integrate information from previous studies including the International Bathymetric Chart of the Southern Ocean Version 2 (IBSCOv2) (Dorschel et al., 2022), and bed topography through Bedmap3 (Pritchard et al., 2024, 2025).

2.2. Terrestrial sampling and observations

Glacial erratics were collected in ice free regions proximal to Vanderford Glacier (Fig. 2), the western flank of Law Dome and the Underwood Glacier (Snyder Rocks), to constrain deglacial timing in the Vincennes Bay and Aurora sub-glacial Basin region. For Law Dome and the Vanderford Glacier, the samples were taken in transects running inshore from near the present day coastline in Vincennes Bay and the Windmill Islands, whereas only one bedrock outcrop was sampled near the Underwood Glacier due to limited accessibility. Sample sites were selected by targeting the tops of local hills above the mid-Holocene high stand (Goodwin, 1993a), with glacial erratics sampled for ^{10}Be cosmogenic exposure dating. For this study, sample sites are denoted by a number (e.g. 582, 458 etc.), with an appended letter denoting samples taken from these sites (e.g. 458a, 458b etc.) (see Appendix A, Section 1.1). Samples from each site were evaluated for glacial clast weathering using a Schmidt Hammer and a visual assessment of the degree of weathering. At some further sites only glacial clast weathering assessment was undertaken (Appendix A; Figure A.1) [dataset] (White, 2021).

2.2.1. Weathering and glacial features

At each sample site, the weathering characteristics of glacial clasts were mapped using the Moriwaki Degree of Weathering (MDoW) index (Moriwaki et al., 1994) and Schmidt Hammer rebounds (Matthews and Shakesby, 1984; Shakesby et al., 2006) to better constrain the relative timing of past glacial retreat. The techniques used are described in White et al. (2009, 2022), with Moriwaki values taken from a range of lithologies at each of the sampling sites and Schmidt hammer measurements from felsic gneiss glacial erratics, to avoid impacts that different lithology can have on the measurements.

2.2.2. Cosmogenic nuclide sampling and analyses of glacial erratics

Sample sites that are considered indicative of the ice expansion and retreat of Vanderford Glacier are Haupt Nunatak, Browning Peninsula, Peterson Island and Holl Island (see Fig. 8). We expect sites on Mitchel Peninsula, Pidgeon Island, Midgley Island and Hollin Island to be more closely linked to the Law Dome system. Samples from Snyder Rocks were collected as to constrain the timing of retreat of Underwood glacier.

Where possible three erratics of cobble size, or greater, were sampled at each site. Samples from each numbered site were taken within ~3 m elevation, and ~20 m radius of each other. We preferentially sampled minimally weathered quartz rich erratics to maximise the yield of quartz for ^{10}Be dating because the minimally weathered samples tend to produce exposure ages that better represent deglaciation timing (White et al., 2009, 2022).

Site and sample locations were recorded using a Garmin e-trex GPS and elevations cross checked against the REMA 2 m Digital Elevation Model (DEM) (Howat et al., 2022), corrected to the EIGEN-6C4 global gravity field model (Foerste et al., 2014). The GPS altitude and corrected REMA elevations were broadly consistent, with the REMA ranging from −5.9 to +6.9 m difference, suggesting that the measured altitude contributed <1% error to the calculated exposure ages. The GPS locations of two sample sites (593 and 594) were manually adjusted using the REMA data to the summits of their respective knolls, as the measured locations were clearly inaccurate upon visual inspection. For these samples, the EIGEN-6C4 corrected REMA grid elevations were used for exposure calculations. Topographic shielding correction was applied using the CRONUS–Earth topographic shielding calculator (Balco et al., 2008), with only minor shielding corrections of <1% [dataset] (White, 2024).

Samples were crushed to 250–500 μm and quartz purified at the University of Canberra following procedures based on (Kohl and Nishiizumi, 1992). For all samples other than 455c, 552c, 593a, and 593BR-1, beryllium (Be) was extracted from the purified quartz at the University of Wollongong following procedures described in Codilean et al. (2023). Samples 455c, 552c, 593a, and 593BR-1 were processed at the Australian Nuclear Science and Technology Organisation (ANSTO) following procedures described in Child et al. (2000) and Fink & Smith (2007). ^{10}Be/^{9}Be ratios were measured using ANSTO's 6 MV SIRIUS Accelerator Mass Spectrometer (AMS) Facility (Wilcken et al., 2017, 2019, 2022). Isotope ratios were referenced to isotope standards KN5-2 and KN5-3, using nominal ^{10}Be/^{9}Be ratios of 8.558×10^{-12} and 6.320×10^{-12}, respectively (Nishiizumi et al., 2007) and ranged between 21.6 ±0.9 and $1039.8 \pm 28.8 \times 10^{-15}$. Background corrections were made using full chemistry procedural blanks (n = 7) between 0.62±0.15 and $3.23 \pm 1.94 \times 10^{-15}$. Final analytical errors in concentrations (atoms/gram quartz) were derived from a quadrature sum of the standard mean error in an AMS ratio, 2% for AMS standard reproducibility and 1% for Be spike assay and other analytical uncertainty such as quartz mass (Appendix A; Table A.1).

Exposure ages (Appendix A; Table A.2) were calculated using the CRONUS-Earth online calculator (Balco et al., 2008) and the LSDn scaling scheme (Lifton et al., 2014). We apply a global calibration dataset for the sea-level-high-latitude ^{10}Be production rate (Borchers et al., 2016), using an Antarctic air pressure correction, rock density of 2.7 g/cm^3 and no topographic shielding.

Exposure ages were calculated assuming no post depositional erosion, which appears appropriate for most of the sample set based on observed morphology, with many samples retaining a morphology indicative of glacial transport and/or glacial polish. An estimated erosion rate of 0–2 mm/kyr (Appendix A; Table A.3), would have a negligible impact on interpretations (e.g. Suganuma et al., 2022; White et al., 2022). However, two samples from Snyder Rocks (593a, 594b) appear considerably more weathered with an erosion rate estimated at 5–10 mm/kyr. This is in line with higher rates seen in previous studies at the Rauer Group and Vestfold Hills (e.g. White et al., 2009, 2022), and likely due to their proximity to the coast and a prevailing marine wind, which we acknowledge could mean an underestimate of these two ages by 1.5–8.8% based on a 5–10 mm/kyr erosion correction.

2.2.3. Radiocarbon analysis of marine fragments in supraglacial moraines

Grounded ice cliffs north of the main Loken Moraines, landwards of the Swain Group of Islands were described by Goodwin (1993b, 1996) and Goodwin et al. (2018), and designated as Ice Cliffs, #254 and #10). These ice cliffs comprise the basal debris-bearing ice that is exposed in marine cliff faces. The exposure reveals an upper and lower, stacked debris-rich ice sequence separated by a folded green translucent ice and light green bubbly-ice sequence. Above the upper debris-rich sequence, a third stacked debris-rich ice sequence emerges beneath a boulder-strewn supraglacial moraine. The green translucent ice was interpreted from stable isotopic stratigraphy, biogenic content, crystallography, and solute chemistry as being marine ice incorporated into the Law Dome ice margin by an overriding of fast ice or a small ice shelf (Goodwin, 1993b; Goodwin et al., 2018). Goodwin (1993b) determined the outcropping fine sandy gravel sediment forming the supraglacial moraine above the cliffs to be saturated marine sediment.

The marine sediments found in these moraines could only have formed in the absence of grounded ice, representing a time of ice retreat beyond present. They were subsequently entrapped in the basal layer of the ice sheet and worked to the surface to form supraglacial moraines via glacio-tectonic folding of the glacial ice (Souchez, 1967; Weertman, 1961), as it pushed up against the inclined bedrock of the northern Windmill Islands during a glacial re-advance (Goodwin, 1996; Chinn, 1989). Thus, we interpret the radiocarbon ages from entrapped carbonaceous fragments as minimum constraints on re-advance of the ice.

The sediment was found to contain shallow marine benthic diatoms together with sponge spicules, coralline algae, *Bryozoan sp.*, *Molluscan sp.* and *Pecten sp.* shell fragments. These were recovered from the northern end of the Loken Moraine at ice cliff 254 (Goodwin, 1993b) (66° 12′ 43.7″ S, 110° 40′ 43.5″ E). This location is a few km seaward of a small subglacial basin, where bed topography is tens to a few hundred metres below modern sea level (Goodwin et al., 2018), and we agree with Goodwin (1993b) and Goodwin et al. (2018) that this material has been subglacially reworked from former marine sediment deposited within this basin.

Six fragments of coralline algae, *Molluscan sp.* and *Pecten sp.* shells approximately 1–2 cm length were sampled from the upper unit in 1988. They were measured for Radiocarbon dating at the ANTARES AMS Facility, in Sydney, Australia using standard carbonate pre-treatment.

3. Results

3.1. Bathymetry

The surveyed area of sea floor revealed widespread glacial landforms. Glacial troughs and large scale lineations are common and have been grouped here based on geographic location and relative timing (see numbered polygons in Fig. 2). Compass bearings are all from true north based on the WGS 84 datum.

3.1.1. Outer continental shelf

The outer group lies toward the continental shelf edge on the north flank of Petersen Bank (Fig. 2; polygon 1). Three different glacial features are observed in the sea floor; lineations, mega-scale glacial lineations (MSGL) and irregular grooves. The lineations are ~2–4 m from peak to trough and up to 50 m wide, oriented at 010°. They are spaced around 100–200 m apart and are between 0.5 and 3 km long (Fig. 3). These lineations are interpreted as the northward expansion of a regional ice stream during a past glacial period, grounded to within 10 km of the continental shelf break (Bennett and Glasser, 2009). We propose the name, Vincennes Bay Ice Stream (VBIS), to refer to the coalescence of ice masses entering Vincennes Bay into a single regional ice stream during glacial periods.

The lineations are overprinted by MSGLs 5–12 m deep and 200–300 m wide, with lengths that are longer than the ships multibeam track (>1.5 km). Some of these are at a similar orientation to the smaller lineations and some differ slightly being orientated at 020°. The overprinting relationship suggest they postdate the smaller lineations and they are consistent with a faster-moving ice stream and relatively higher basal shear stress (Bennett and Glasser, 2009; Jamieson et al., 2016; King et al., 2009; Livingstone et al., 2016).

Both classes of linear features are overprinted again by irregular grooves that we interpret as being formed through iceberg scouring. These grooves are 2–6 m deep and 50–100 m wide. The iceberg scours are more common in depths shallower than 440 m, whilst the lineations are prevalent in the deeper regions (440–460 m).

To the west of Petersen Bank there is a ridgeline evident in the IBSCOv2 and Bedmap3 data (Fig. 3) (Pritchard et al., 2024; Dorschel et al., 2022). A cross section of this feature reveals a profile similar to large GZW's seen in other locations around Antarctica such as Prydz Bay (O'Brien' et al., 1999), suggesting a possible glacial origin. Whilst these datasets are lower resolution (500 m) compared to the multibeam bathymetry, due to the scale of this ridge feature, we consider it adequate for these broadscale interpretations. Further, the transect depicted in Fig. 3c is in a part of Vincennes Bay where there is considerable single beam bathymetry data constraining the IBSCOv2 interpolations, allowing for reasonable depth uncertainty, again due to the scale of the feature (see Appendix B, Section 1.)

3.1.2. Inner continental shelf

Directly in front of the Vanderford and Adams Glacier calving fronts there are a series of deep glacial troughs carved into the bedrock to a depth of over 2000 m (Fig. 4a). From these troughs, the bathymetry slopes upwards to the NW (Reverse slope) where it rises to ~1000 m depth over ~70 km. Lineations mark the bedrock and unconsolidated sediment within these troughs. In the troughs associated with Vanderford Glacier the lineations lie at depths of ~1300–1600 m and are orientated at 300°. They are ~10 m in height, >2 km long, and 0.5–1 km apart. Within the Adams Glacier trough, lineations (3–4 m high, 1–2 km long) are less common and follow the general orientation of the trough, varying from 305 to 325°.

A transition from bedrock to unconsolidated sediment is evident ~40–50 km NW from the Adams Glacier calving front (Fig. 4a), where the water depths decrease considerably and the palaeochannel becomes unconfined. MSGLs 5–10 m high, >5 km long and 50–150 m wide become common, with bedrock mega-grooves (Bennett and Glasser, 2009) and meltwater channels similar to those observed in McCormack et al. (2023) evident in topographic highs, that we interpret as protruding bedrock (Fig. 4b–d). Drumlins up to ~60 m high and 200–400 m wide are also observed to the north of the Vanderford Glacier. These features have long axes orientated between 321 and 337° with a general pattern of veering slightly West (Fig. 4c–e).

3.1.3. Petersen Bank

Petersen Bank is a shallow region sitting off the northern flank of Law Dome, extending to the continental margin and with depths ranging

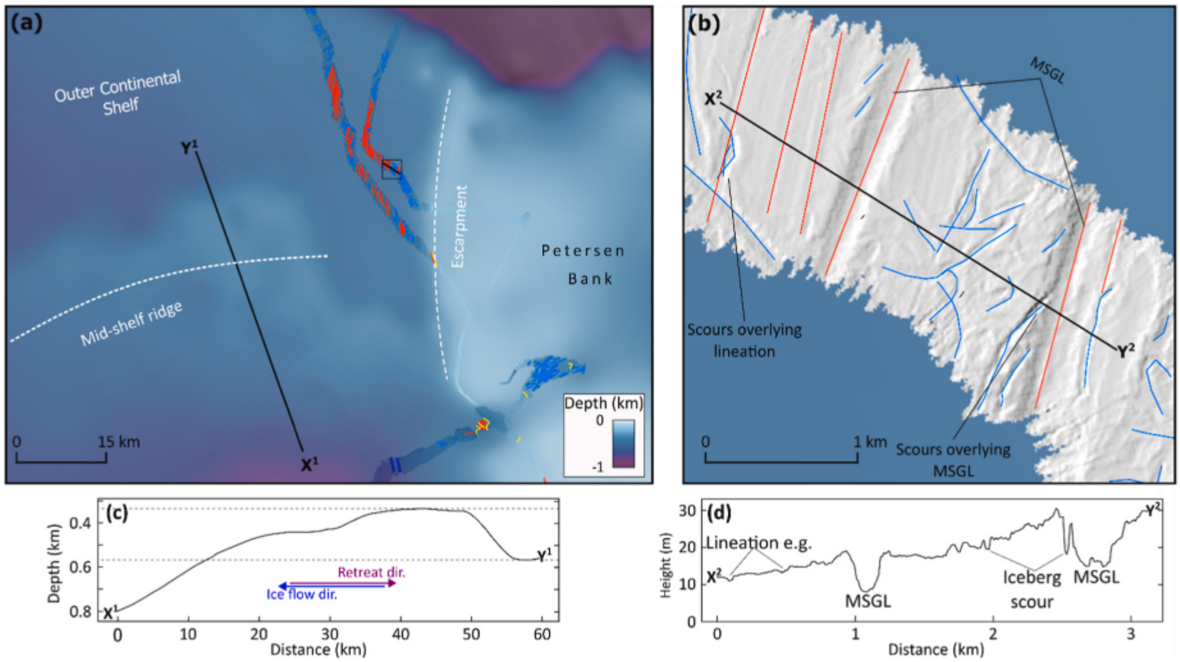

Fig. 3. Bathymetric features of the Outer Group (1). Lineations are represented with **red lines**, **blue lines** are iceberg scours and **yellow lines** are moraine features. **Black lines** are depth profiles. Panel **(a)** shows the regional context, and two large scale features (**white dotted line**) that contributed to broad scale glacial retreat dynamics of a regional ice stream. Panel **(b)** is the inset and gives closer view of glacial features. Panel **(a)** includes data from IBSCOv2/Bedmap3 dataset (Dorschel et al., 2022; Pritchard et al., 2024) and both panels **(a)** and **(b)** include multibeam bathymetry data from the 2021–2022 ANARE Antarctic season [dataset] (Commonwealth of Australia, 2022) referenced to WGS 84. Multibeam data in panel **(b)** is shown in black and white hillshade to better highlight the observed features. Panel **(c)** depth profile utilises the IBSCOv2 (Dorschel et al., 2022) data integrated into the Bedmap3 package (Pritchard et al., 2024) and panel **(d)** depth profile utilises the multibeam data. (For interpretation of the references to colour in this figure legend, the reader is referred to the Web version of this article.)

from 50 to 350 m. Two deep troughs are evident on the western margin of Petersen Bank, which descend W-SW, towards the centre of Vincennes Bay and the deep palaeo-Vanderford trench (Fig. 2; polygon 3, Fig. 5). The multibeam data support previous seismic mapping by Harris et al. (1997), who interpreted the northern valley as a U-shaped valley of glacial origin and the southern valley as an asymmetrical valley that demarcates the boundary of the deeply eroded basement rock of the inner continental shelf and the younger sedimentary basin of the outer continental shelf. The northern U-shaped valley has step-like features in the south valley wall, interpreted by Harris et al. (1997) as being incised into the valley sides.

A depth profile along one of the glacial troughs reveals a series of glacial features including moraines, lineations and a GZW and confirm the presence of enough grounded ice on Petersen Bank capable of forming ice streams of a considerable size. This glacial trough runs in a NE-SW orientation stretching from Petersen Bank (~250–350 m depth) to the palaeo-Vanderford trench (~750 m depth) (Fig. 5a–e). Lineations along the profile are subtle at 1–3 m high, 0.3–1.5 km long and oriented at 260°, suggesting active ice flowed from the high ground on Petersen Bank down the trough toward to southwest. The ice stream terminated at ~800 m depth, as shown by a GZW (Fig. 5c and d).

The retreat of ice through the trough is characterised by multiple sections of reverse and normal sloped bed. The lower section of the trough gently rises from ~800 m to ~450 m depth towards the base of Petersen Bank (NE), over ~20 km. A lack of moraine or other recessional features is indicative of a rapid single phase of retreat over this section. At ~450m depth a reverse slope leads to the edge of the Petersen Bank escarpment, where a series of recessional, stacked moraines (Fig. 5b–d) are present over a stretch of around ~7.5 km. The bathymetry then rapidly rises to the top of the escarpment (~250 m depth) before once again transitioning to a reverse slope and a depth of ~350 m. Along this section of reverse slope, two recessional moraines are observed, separated by ~10 km, again indicative of a relatively rapid retreat. Of note, in depths greater than 700 m, there are several linear MSGL/drumlin like features crossing the width of the bathymetry swath (Fig. 5a–c, d), perpendicular to the direction of ice flow from Petersen Bank. These are considerably larger in scale than other glacial features seen on the transect and may be remnants from an expanded S-N flowing VBIS that were later smoothed by ice flowing from Petersen Bank.

All GZW's are of similar size, ~10 m high and about 200–500 m wide, with a gentle slope toward the NE and a steeper face to the SW. There is a feature at the Petersen Bank end of the bathymetry profile (Fig. 5c), which corresponds to the lateral moraines identified in seismic depth profiles by Harris et al. (1997). Heavy iceberg turbation is also present on this part of Petersen Bank, possibly due to iceberg movement from east to west, grounding on Petersen Bank as the depth decreases from 350 to 250 m.

Further to the south, Petersen Bank becomes particularly shallow (80-50 m depth), with two distinct groupings of subtle lineations (1–3 m high) present, one varying between 160 and 178° and the other grouping at 290°. The second U-shaped feature cuts through the shallows to ~350 m depth. This trough is much rougher in profile, suggesting bedrock is present, with some subtle lineations on the northern trough wall.

3.1.4. *Law Dome shallows*

This data set builds on a previous bathymetric study of the shallow bays that flank Law Dome (Carson et al., 2017) extending further west into the Vincennes Bay (Fig. 6). Lineations are present but uncommon and follow a roughly E-W direction within the confines of local troughs and channels. Moraine features are also present in the bathymetric lows, mostly found in several close-set groupings, which become less common further from Law Dome. Moraines are mostly 2–4 m high and asymmetric in shape, most of which have a steeper distal (downstream of flow) slope.

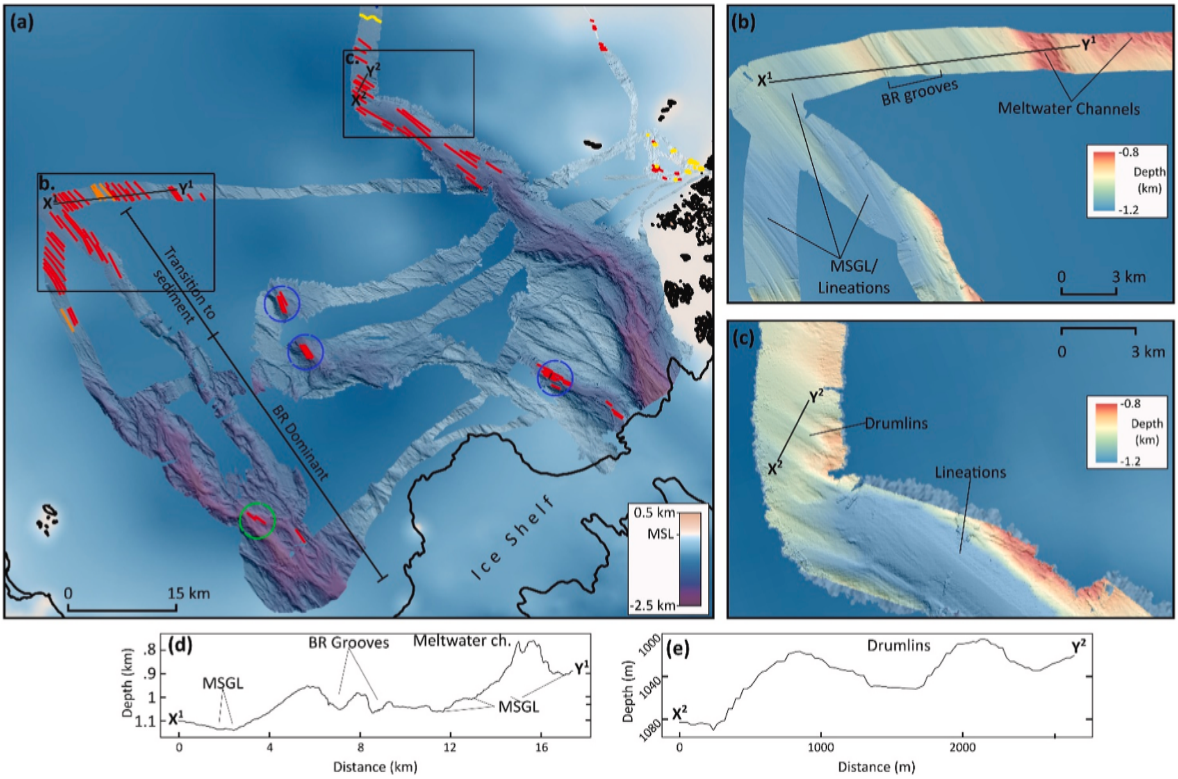

Fig. 4. Inner continental shelf bathymetry. Panel **(a)** shows the bathymetry data of the over-deepened glacial troughs. **Red lines** are lineations, **orange lines** are bedrock grooves and depth profiles are **black lines**. Panel (**b**) is a close up of the bedforms within the unconsolidated material and protruding bedrock highs and the depth profile represented in panel (**d**). Panel (**c**) is a close up of the drumlin features and lineations north of the Vanderford Glacier, with the associated depth profile shown in panel (**e**). **Coloured circles** are smaller scale lineations in sediment beds within the troughs. **Green circles** are 3–5 m high and 50–100 m wide and ~2 km long. **Blue circles** are 10–15 m high, ~100 m wide and >2 km long. The base maps in panel **(a, b** and **c)** include data from the IBSCOv2/Bedmap3 dataset (Dorschel et al., 2022; Pritchard et al., 2024) and multibeam bathymetry data from the 2021–2022 and 2023–2024 ANARE Antarctic seasons [dataset] (Commonwealth of Australia, 2022, 2024) referenced to WGS 84. All depth profiles are created from multibeam data. (For interpretation of the references to colour in this figure legend, the reader is referred to the Web version of this article.)

3.2. *Weathering of terrestrial glacial sediments*

A general trend observed in both the MDoW index and Schmidt hammer rebound measurements is that glacial clasts in locations closer to the ocean are more weathered than those close to, or at the ice margin (Fig. 7). These weathering measurements are often indicative of relative deglaciation timing, but here they need to be interpreted with caution, as this weathering pattern is confounded by windblown sea salt, which has been found to increase weathering rates by at least an order of magnitude in coastal oases around other parts of East Antarctica (Gore and Leishman, 2020; Kiernan et al., 2009; White et al., 2022).

Near the modern day Vanderford system, Haupt Nunatak (site 1013/1014) yielded the least weathered glacial erratics (MDoW:110–125; Schmidt rebounds: 44.4 ± 6.8). In contrast, Browning Peninsula, Holl and Ford Islands were considerably more weathered (MDoW: 290–348; Schmidt: 28.1 ± 5.9–32.1 ± 7.3). Samples from the western flank of Law Dome show a similar pattern, with samples closer to the ice margin at Kros and Loken shear moraines (Fig. 7), and the smaller ice cored moraine on Bailey Peninsula (sites 511 and 522) being less weathered (MDoW: 5–154; Schmidt: 40.7 ± 9.5–48.8 ± 7.4) compared to the peninsulas (Mitchel, Bailey, Clark and Robinson Ridge) and islands (Hollin and Pidgeon) (MDoW: 120–348; Schmidt: 26.6 ± 5.7–39.6 ± 7.1).

Some sample sites on Mitchel and Clark peninsulas (sites 455, 458, 481) are situated further from the ocean than other peninsula samples, proximal to the Law Dome ice margin. These yielded intermediate MDoW (105–160) and Schmidt (40.2 ± 11.1–45.6 ± 9.9) scores.

Within the shear moraines, there is typically an inner and outer moraine with visibly different weathering characteristics (Goodwin, 1996), which is reflected in the Moriwaki index and Schmidt hammer rebound measurements for these features (Fig. 7).

3.3. *^{10}Be exposure ages*

Generally, the ^{10}Be exposure ages present a sequence of progressively younger exposure ages toward the modern ice margin on each of the transects. Where replicate samples have been analysed from a single site (with an identical expected deglaciation timing), erratic ages are largely within a few hundred years of each other, and within or close to 2 σ analytical uncertainties. However, there is clear evidence of scatter within some sites, particularly at 458, 834 and 838 where samples disagree by up to 2–5 ka (and are discordant at >5 σ internal uncertainties) within a single site. While the degree of weathering of each sample was recorded (Appendix A; Table A.3), there were no clear trends within a site between increased degree of weathering of erratics and their exposure age. In these environments this scatter is typically attributed to inheritance due to cosmic-ray exposure prior to the latest deposition (e.g. White et al., 2011, 2022). Thus, for interpreting deglaciation timing we assume the minimum age at each site best represents the deglaciation age.

The ^{10}Be exposure ages suggest a similar deglaciation timing across the Vincennes Bay region, with the outer Windmill Islands yielding ages of 9.7–11.1 ka. Ice marginal samples from circa Vanderford and Law Dome also yield similar ages (Vanderford: 8.6–9.3, Law Dome 8.5–10.0 ka), suggesting the retreat across the Windmill Islands and Peninsulas occurred during a ~1000 yr period. Similarly, sample sites from the

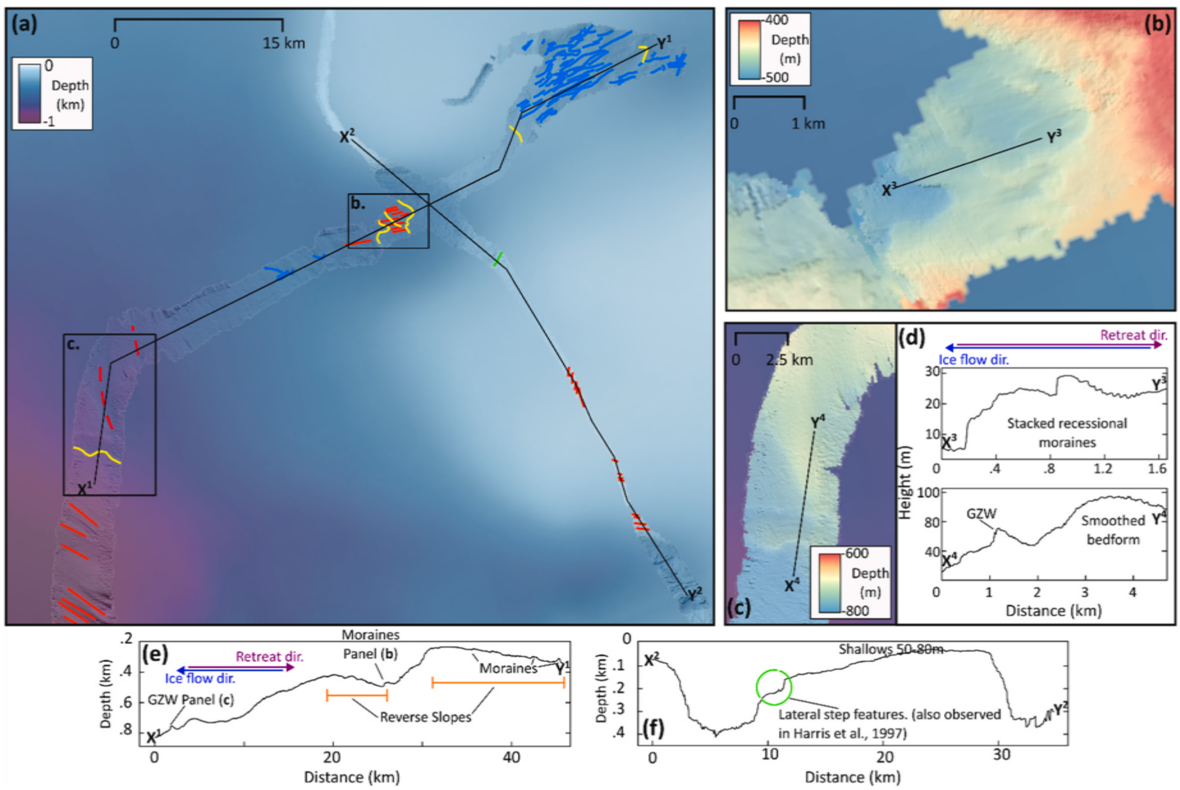

Fig. 5. Petersen Bank palaeo ice stream bathymetry. Panel **(a)** base map shows Petersen Bank bathymetry. Lineations are **red lines**, moraines and GZWs are **yellow lines** and **dashed red lines** show smoothed linear features possibly indicating past ice direction. **Blue lines** represent iceberg scours, whilst the **green** is the lateral step also identified by Harris et al. (1997). Panels (**b**) and (**c**) offer close up imagery of key bedform features within the Petersen trough. The associated depth profiles can be seen in panel (**d**). Panel **(e)** is a depth profile of a cross section along the entire Petersen Bank glacial trough, terminating at the edge of the over-deepened troughs north of the Vanderford Glacier. Panel **(f)** depth profile cuts across the Petersen trough, and the shallows observed on Petersen Bank. Panel **(a)**, (**b**) and (**c**) data are from IBSCOv2/Bedmap3 dataset (Dorschel et al., 2022; Pritchard et al., 2024) and multibeam bathymetry data from the 2021–2022 ANARE Antarctic season [dataset] (Commonwealth of Australia, 2022) referenced to WGS 84. (For interpretation of the references to colour in this figure legend, the reader is referred to the Web version of this article.)

Snyder Rocks (Underwood Glacier) produced exposure ages of 9.3–10.0 ka.

Inland of the current grounding line Haupt Nunatak, adjacent to the Vanderford Glacier, was exposed at ~3.7 ka. At Law Dome, exposure ages from samples collected on a small moraine noted by Goodwin (1996) on Bailey Peninsula (Bailey Moraine; sample site 552) suggest more recent exposure of 1.1–1.8 ka. We note that these are likely minimum ages due to the location being an ice-cored moraine and therefore potentially mobile terrain.

3.4. *Shell and coralline algae ^{14}C ages*

The six shell and algal fragments returned radiocarbon ages of 3.6–5.4 ^{14}C kyr BP , and we interpret them as representing a single period of retreat of the grounding line inland of the present day during the mid-late Holocene. However, the reworked nature of these fragments complicates precise calibration to calendar ages. While the six shell fragments analysed are clearly marine in origin, the habitat of these species ranges from a few metres below sea level to ~125 m for coralline algae and several hundred metres for Molluscan sp. and Pecten sp. The radiocarbon reservoir age in these environments is presently disparate, varying from a few hundred years in well-ventilated shallow marine inlets around Windmill Islands (Small et al., 2025), to between 900 and 1700 years (median ~1200 years) in more open marine environments (Berg et al., 2020a; Berkman and Forman, 1996; Divola et al., 2024). Thus we present both end-members calculated via Calib 8.2 using the Marine 20 calibration dataset (Heaton et al., 2020). We interpret the results to indicate that grounded ice must have retreated inland of the present day ice cliff location prior to 5.7–4.5 cal ka B.P (i.e. the full potential calibrated age range of sample 254/04/01), with re-advance to the present position occurring - after 3.4–2.3 cal ka B.P (254/04/06, Table 1, Fig. 8).

4. Discussion

4.1. *Deglaciation pattern and timing*

The combination of evidence from marine geomorphology, and terrestrial chronology suggests the VBIS underwent four main phases of deglaciation (Fig. 9). Phase 1 (undated, but predates all other phases) where the grounded ice extended to the shelf-break and a subsequent rapid retreat. Phase 2 (pre Holocene to ~10 ka) represents the most recent stable ice configuration at the mid-shelf ridge followed by retreat of marine based ice along major overdeepened troughs, which isolated the independent ice centre on Petersen Bank and Law Dome's western flank extending through the Windmill Islands. Phase 3 (~10–8.5 ka): Retreat of ice centre on Petersen Bank and of western Law Dome close to modern limits. Phase 4 (mid-to-late Holocene ~6–2 ka): Minor Holocene retreat and adjustments to the ice margin.

4.1.1. *Phase 1: outer shelf extent and retreat*

The lineations and MSGLs on the outer continental shelf NW of Petersen Bank indicate grounded ice was present to at least 10 km from the continental shelf break, prior to deglaciation (>10 ka). The size of the lineations suggest a large ice-stream (Bennett and Glasser, 2009; Clark, 1993; O'Brien et al., 2016) was present at that time, albeit

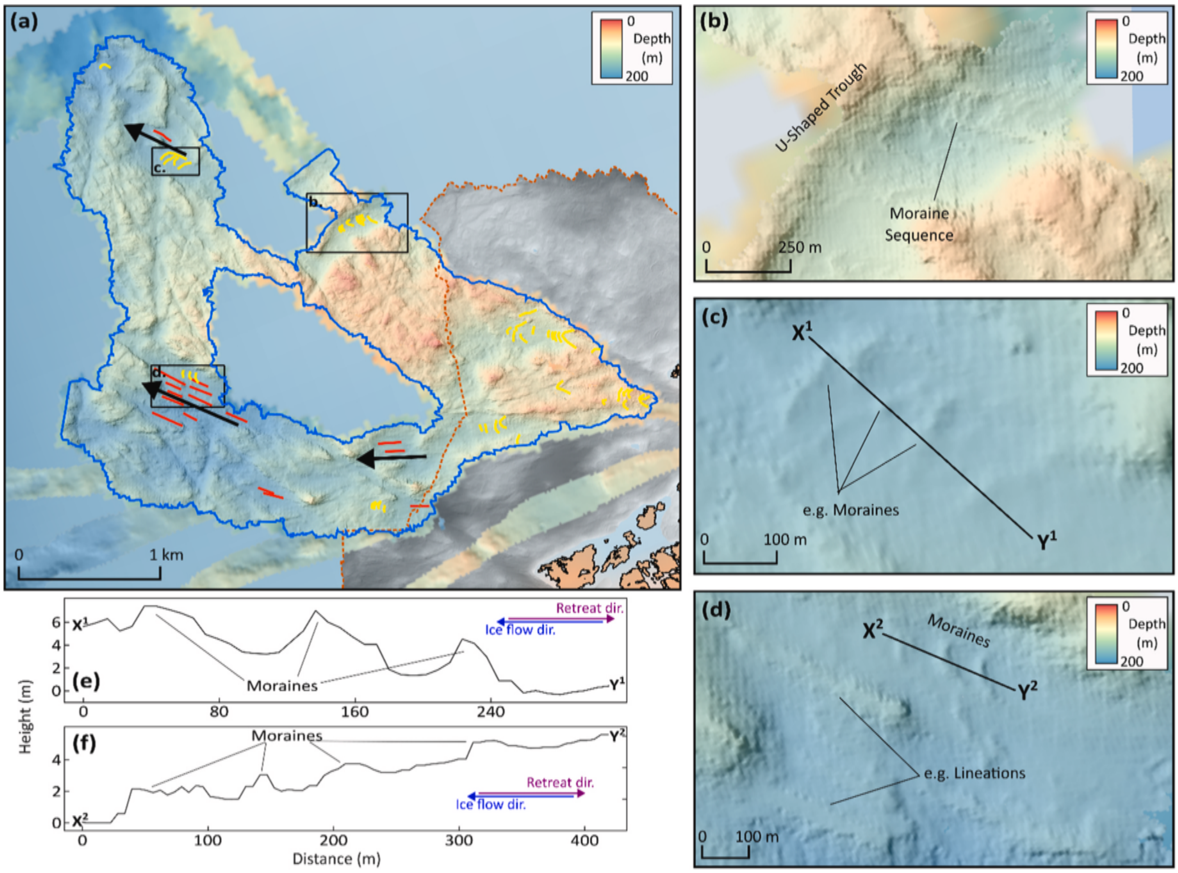

Fig. 6. Law Dome shallows bathymetry**.** Panel **(a)** base map shows bathymetry of the shallows to the west of Law Dome. **Red lines** are lineations, **yellow** are moraines and **black arrows** are generalised palaeo-ice flow direction. Panel (b) is a close up view of a U-shaped glacial trough, with a moraine sequence evident within. Panel (c) and (d) are close up views of recessional moraine features typically observed in the area, with associated depth profiles seen in panel (e) and (f), respectively. Panel (**a**) base layer data from IBSCOv2/Bedmap3 dataset (Dorschel et al., 2022; Pritchard et al., 2024). The multibeam bathymetry data **outlined in blue** is a 5 m DEM from the 2021–2022 ANARE Antarctic season [dataset] (Commonwealth of Australia, 2022), also seen in the close ups in panels (b), (c) and (d). Greyed out bathymetry data with orange dashed outline is a 1 m DEM [dataset] (Carson et al., 2016) analysed in (Carson et al., 2017). All referenced to WGS 84. (For interpretation of the references to colour in this figure legend, the reader is referred to the Web version of this article.)

relatively moderate/slow moving with low basal shear stress conditions. The MSGLs that overly the lineations are consistent with a relatively fast-moving ice (Jamieson et al., 2016; King et al., 2009; Livingstone et al., 2016), which we suggest is related to the thinning and acceleration of the VBIS, possibly due to the loss of the ice shelf, or changes in mass balance, subsequent to the retreat of the system.

The western flank of Petersen Bank is a N-S running escarpment ~250 m high running roughly parallel to the lineations and forms a natural barrier that would have confined the eastern edge of the ice stream. A lack of glacial features atop the escarpment further support this (Fig. 3). Ice was grounded on Petersen Bank, either as a northward expansion of Law Dome or an independent ice centre, as indicated by the observed glacial features (Section 3.1.3). More data are needed to confirm whether it was grounded to the continental shelf break, however the geometry of Petersen Bank suggest that it is likely (Fig. 3).

Given a lack of dated material from the outer continental shelf, we are unable to say whether the presence of grounded ice in phase 1 was from the LGM or a prior, larger glaciation, but these features clearly predate all other glacial events thus far recognised on the shelf.

4.1.2. Phase 2: mid-shelf and over-deepened troughs

4.1.2.1. Glacial setting. In the mid-shelf region, a >50 km long ridge line is observed in single point bathymetry and is also present in modelled bed topography data, shoaling to ~350 m below modern sea level (Fig. 3a) (Pritchard et al., 2024; Dorschel et al., 2022). The large ridge feature arcs southwest towards the centre of Vincennes Bay, with substantially over-deepened topography landward of the feature. This topographic geometry suggests that this would have been a pinning point for the grounding line during ice retreat from the outer continental shelf. While the cross section and large-scale form resembles a large GZW (O'Brien et al., 1999) (Fig. 3b), further research to determine if this is indeed the case is needed.

To the southeast of the mid-continental shelf ridgeline, the seabed is relatively flat and unconfined, though MSGLs show that a broad ice stream was grounded a minimum of 75 km northwest of the present-day coastline and likely much further into the bay. The topography slopes back from the ridge line towards the southeast and the various modern outlet glaciers draining into Vincennes Bay. Multibeam data reveal that the flat and unconfined bed transitions to a series of deep glacial troughs ~50 km northwest of the modern day Vanderford and Adams Glaciers. A recent gravity inversion bathymetry dataset (Bird et al., 2025) also shows how these deep glacial troughs transition to a flatter unconfined bed but also shows that the ice flow followed more subtle troughs north of the Vanderford Glacier and northwest from the Adams Glacier trench. Although we lack multibeam data offshore from Underwood Glacier, McMahon et al. (2023) observed a deep trough in this area utilising data from Elephant seal dive depths captured with Satellite Relay Data Loggers (SRDL). Importantly, the reverse sloped bed and deep troughs of the inner continental shelf provide a suitable environment for rapid retreat due to MISI (Jones et al., 2015; Schoof, 2007).

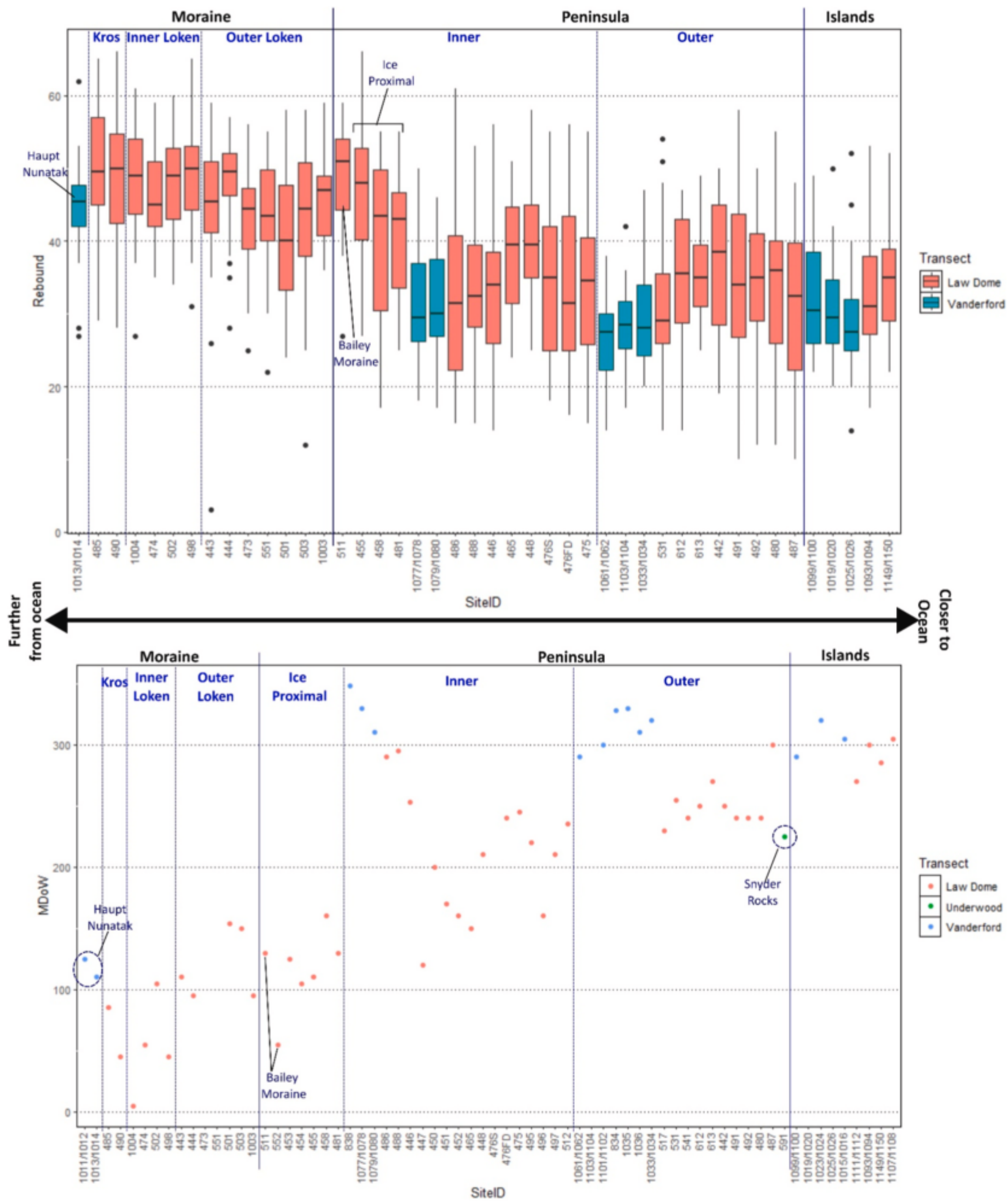

Fig. 7. Boxplot of Schmidt Hammer rebound measurements (top panel) and scatter plot of MDoW scores (bottom panel). Sample sites are divided into landform classes and proximity to the ocean. Boxplot and point colours are indicative of which modern system likely dominates the glacial processes for that site. Of note, Haupt Nunatak is at the interface of two systems, likely dominated by the Vanderford during LGM and Law Dome through the Holocene, or a combination of the two as discussed in sections 4.1.4 and 4.3. (For interpretation of the references to colour in this figure legend, the reader is referred to the Web version of this article.)

4.1.2.2. Retreat timing. Geochronological constraints on ice retreat during Phase 2 are largely from nearshore and onshore of the Windmill Islands. Here, onshore ^{10}Be exposure dating reveals that the outer Windmill Islands (e.g. Holl, Hollin and Midgley) were ice free by 10.5–10 ka and Snyder Rocks by 9.5–10 ka (Fig. 8). Dates from these sites, which are located within the main trunk of the former VBIS, constrain its retreat close to modern ice extents at the Vanderford and Underwood Glaciers. These ages are consistent with the onset of biogenic sedimentation in marine inlets from Peterson Island and Browning Peninsula (~10.5 ka) (Cremer et al., 2003; Kirkup et al., 2002; Small et al., 2025). Two marine cores described in Harris et al. (1997) and dated by Harris (2000) provide the only current age constraints on deglaciation (~8.5 and 11.3 ka) within the deep troughs afront the Vanderford Glacier (Fig. 8). Whilst these ages are broadly consistent with the new exposure ages and minimum constraints from other studies, they have multi-thousand year reservoir corrections (4 ka to 9ka determined from surface sediment radiocarbon ages) and thus should be considered with caution.

Taken together, the chronologies indicate widespread grounding line retreat to the inner continental shelf by ~10 ka. Additionally, there is an absence of grounding zone features between the large mid-slope ridge and the over-deepened troughs that front the major modern outlets of the Vanderford and Adams glaciers. Combined with the reverse bed slope inboard of the mid-slope ridge we suggest that grounding line retreat to these dated positions likely occurred in a single phase, with the termination of this event occurring at ~10 ka, suggestive of a rapid retreat possibly due to MISI.

Table 1
^{14}C age and calibration for marine shell fragments found at Ice Cliff 254.

Field Code	Lab Code	Sample Type	Conventional ^{14}C Age	Calibrated age: local/shallow marine Delta-R = 0 (cal yr BP)	Calibrated age: regional/deep Delta-R = 650 (cal yr BP)
254/04/01	OZ1786	Coraline Algae	5408 ± 49	5664–5489	5087–4528
254/04/02	OZ1787	Coraline Algae	5028 ± 49	5268–5061	4617–4051
254/04/03	OZ1788	Mollusc Sp. Shell fragment	4863 ± 64	5052–4830	4401–3833
254/04/04	OZ1789	Mollusc Sp. Shell fragment	5339 ± 59	5604–5423	4995–4435
254/04/05	OZ1790	Pecten Sp. Shell fragment	3592 ± 62	3422–3227	2796–2275
254/04/06	OZ1791	Pecten Sp. Shell fragment	3630 ± 62	3460–3263	2835–2315

4.1.3. Phase 3: Law Dome shallows and Petersen Bank

Whilst the main trunk of the VBIS had retreated close to modern ice margins by ~10 ka, ice was likely still present on shallows flanking Law Dome and Petersen Bank, as indicated by the presence of an active flow corridor from Petersen Bank overlying palaeo glacial features from the VBIS main trunk, and the similar geometry between Petersen Bank and the Law Dome shallows (Fig. 5).

The evidence of a smaller scale flow corridor running from Petersen Bank to the southwest into Vincennes Bay overprints features formed by the larger VBIS (Fig. 5) indicating that ice persisted on Petersen Bank after the main trunk of the VBIS had retreated. Deglacial moraines are clustered in areas of a prograde bed, with much larger distances between them on areas of reverse slope, suggesting a variable rate of retreat onto the bank.

To the west of Law Dome, the bathymetry follows a shallow prograde slope away from the current ice margin through several palaeo-glacial valleys that run east-west through the Windmill Islands. The shallow slope falls sharply into the deep glacial trench afront the Vanderford Glacier ~10–15 km west of the Law Dome ice margin. Retreat of the ice margin toward Law Dome occurred progressively through the submerged glacial valleys, leaving closely spaced moraines which are increasingly common closer to Law Dome (Fig. 6) (Carson et al., 2017). This suggests a more rapid retreat across the outer Windmill Islands, slowing as the ice retreated through the more confined and shallower areas among the peninsulas on Law Domes western flank. Closer to the current ice margin the moraines are roughly equidistant suggesting monotonic retreat over this area. Of note, U-shaped valleys and striae on the Frazier Group of Islands ~16 km west of Law Dome suggest expansion of the eastern flank of the VBIS at least partially covering the shallows (Goodwin, 1993a). Somewhere between here and the Outer Windmill Islands is likely the maximum extent of Law Dome during this phase.

Our new exposure ages indicate that Law Dome ice retreated from the outer Windmill Islands to close to the modern margin in <1 kyr, by ~9–8.5 ka (Fig. 8). Given the number of moraines (70–100), and the limited time available (~<1 kyr) each of these features likely formed in ~10 yrs and could potentially represent annual retreat cycles closer to the modern margin as noted by Carson et al. (2017). This rate of retreat is supported by the weathering characteristics of the glacial erratics sampled over most of the Windmill Islands and Peninsulas, with little discernible difference among them (Fig. 7). It is also consistent with penguin colonisation on Bailey Peninsula at 8.9 ka (Emslie and Woehler, 2005) and a transition to more saline conditions in Beall Lake starting at ~9 ka (Roberts et al., 2004). It is worth noting that a recent re-calibration of the Beall Lake core puts the transition to saline conditions at 10.2 ka (Small et al., 2025), which may indicate an even more rapid rate retreat of ice through the outer Windmill Islands, slowing only once constrained by the shallows and peninsulas flanking Law Dome (e.g. Mitchel, Bailey, Clark). It is unclear how long ice remained on Petersen Bank based on the current evidence, however assuming it mirrored the retreat of the Law Dome margin to close to its modern position by 9–8.5 ka we suggest that Petersen Bank was also ice free by this time.

4.1.4. Phase 4: secondary ice margin adjustments - Windmill Islands

Exposure ages from the Bailey Moraine (1–1.8 ka), and the ^{14}C ages from shell fragments incorporated into advancing basal ice and now outcropping in the supraglacial moraine at Ice Cliff 254 (~5.7–2.3 cal ka BP) evidence late-Holocene changes in ice extent of the north-western margin of Law Dome. Similar mid to late-Holocene changes were concluded in Goodwin (1996), attributing the Bailey Moraine feature to a readvance and subsequent retreat of Law Dome during this period. The absence of cosmogenic ages spanning this period, combined with the reworking of mid to late-Holocene marine shell fragments suggests that the Law Dome ice margin was inland of the present day, overlying small sub-sea level basin (Appendix B; Figure B.2, Transect A) from ~5.7 to 2.3 ka, a phenomenon also seen around the Antarctic margin through the Holocene (e.g. Balco et al., 2023; Johnson et al., 2022; Jones et al., 2022; Okuno et al., 2025; Small et al., [preprint]).

Recently, deglacial moraines in Law Dome shallows were also attributed to this event (Carson et al., 2017), however the new cosmogenic ages presented in this study don't evidence a readvance of that magnitude. Sample sites 455 (9.9–8.5 ka exposure) and 458 (12.5–10.0 ka exposure) sit within 2 km of Loken Moraine and at a lower elevation suggesting any ice advance was limited to within that extent. As per Goodwin (1996), we interpret the Bailey moraine as the terminal moraine of the ice advance and assume that the oldest (1.8 ka) exposure age represents a minimum age due to the ice-cored moraine being a mobile landscape feature. This constrains the most recent Holocene readvance as culminating at or before 1.8 ka. We suggest that the recessional moraine features observed by Carson et al. (2017) represent the final stages of post-LGM deglaciation in the early-Holocene.

Haupt Nunatak lies ~50 m above the elevation of the current nearby-surface of the Vanderford Glacier, and within 1 km of the Law Dome margin (Appendix B; Figure B.2, Transect B).The outcropping group of nunataks present smoothed bedrock and lineations in the same orientation (335°) as the Vanderford Glacier's flow (Appendix A; Figure A.3), and so it is likely that an expanded Vanderford was the main cause of burial through the LGM. The exposure ages (~3.7 ka) from Haupt could be attributed to a secondary phase of retreat or ice lowering during the mid to late-Holocene climatic optimum (Goodwin, 1998; Morgan et al., 1997), or a continuation of the main phase of retreat of the Vanderford Glacier post-LGM.

As the main phase of deglaciation was quite rapid and there are several thousand years of difference between Haupt Nunatak exposure ages and the inner Windmill Island samples, it is unlikely that this was the case. Furthermore, there is no clear evidence of a coincident retreat from Peterson Island or Browning Peninsula, which would be expected from a substantive retreat and thinning of Vanderford Glacier.

Alternatively, given the potential for a small amount of inheritance in erratics from the region, as suggested by the ~2 ka scatter in ages across the deglacial, this age may be an over-estimate. If this is the case, then the timing may be closer to the late-Holocene readvance of Law Dome (Goodwin, 1996), also evidenced by the youngest marine shell fragment from Ice Cliff 254 (3.4–2.3 cal ka BP), or subsequent retreat of Law Dome seen at Bailey Moraine (1.8–1.1 ka). Further work is required to conclusively determine what part of the Law Dome retreat/advance

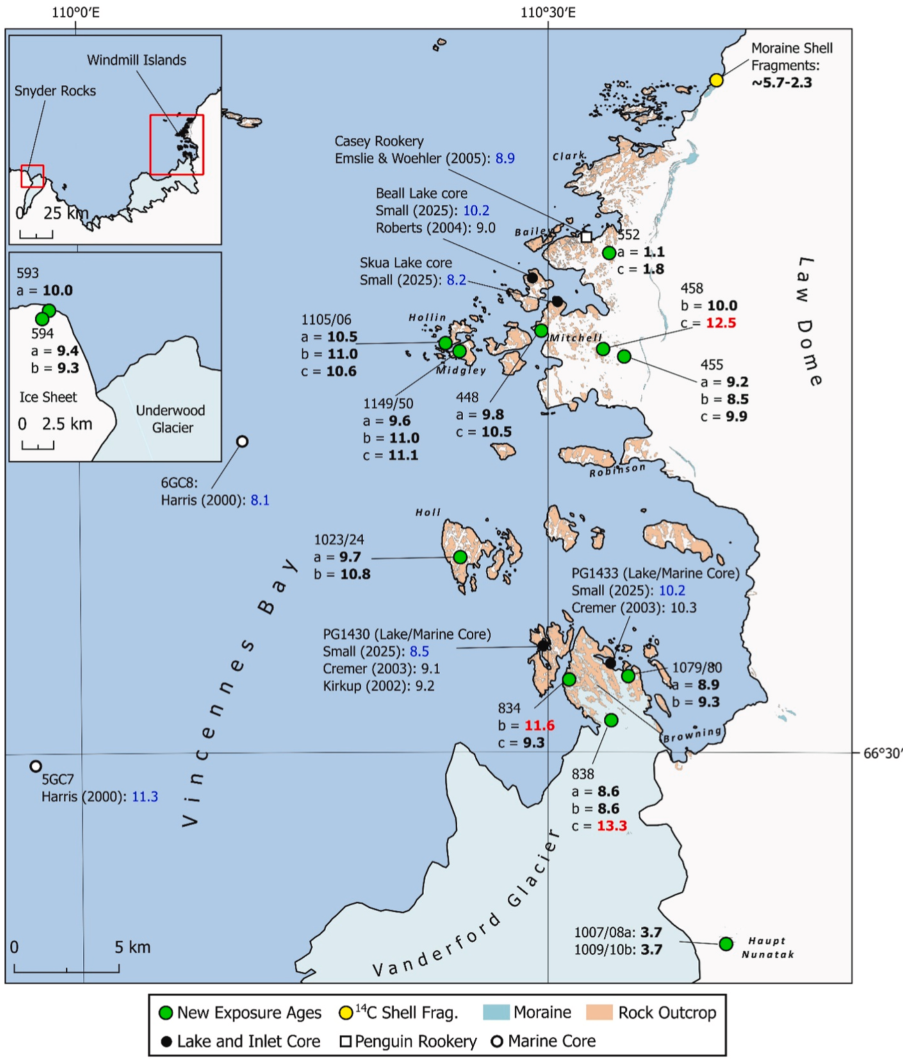

Fig. 8. ^{10}Be and ^{14}C ages in Vincennes Bay. Main map shows the Windmill Islands and the lower inset, Snyder Rocks. Red numbers differ from similar samples (i.e. grouped by geographic similarity and distance from the grounding line of either the Vanderford Glacier and Law Dome), by greater than 2σ uncertainty. Blue numbers are the most recent interpretations of minimum age constraints from previous studies, dated via radiocarbon from biogenic proxies. All ^{10}Be ages are in ka and ^{14}C ages in cal ka BP, using the reported calibrated and corrected ages applied in the original studies (Cremer et al., 2003; Emslie and Woehler, 2005; Harris, 2000; Kirkup et al., 2002; Roberts et al., 2004; Small et al., 2025). (For interpretation of the references to colour in this figure legend, the reader is referred to the Web version of this article.)

cycle the Haupt Nunatak deglaciation was synchronous with, noting we present and discuss a possible scenario later in Section 4.3.

4.2. Glacial retreat around the EAIS margin

Previous studies have suggested that subglacial basin and channel topography are key drivers in continental ice mass loss, with basins that are largely grounded below sea level at a greater risk of early and rapid deglaciation (Morlighem et al., 2020; Stokes et al., 2022). Whilst modern measurements of ice streams in these basins support the idea (Pelle et al., 2020; Picton et al., 2023; Stokes et al., 2022), the palaeo record is still emerging and has been missing key records from over-deepened sectors of the ice sheet.

Presently, the most consistent evidence available for sector-based comparisons is the point at which the grounding line retreated to its modern position, following the main phase of deglaciation post-LGM. This timing varies by sector, occurring at ~5–7 ka at Dronning Maud (Suganuma et al., 2022) and Enderby Land (Kawamata et al., 2020; White and Fink, 2014; Yamane et al., 2011), at ~12 ka in Mac Robertson Land (Mackintosh et al., 2011, 2014), Bunger Hills (Gore et al., 2001) and the Amery Oasis (White et al., 2011) and as early as 14 ka at the Rauer Group in Eastern Prydz Bay (White et al., 2022) (Fig. 10). In comparison, the main phase of retreat of the Vincennes Bay regional ice stream was largely complete ~10 ka when the outer Windmill Islands were exposed (Fig. 8).

Although the timing of stabilisation at Windmill Islands (~10 ka) falls within the range of other regions (6–14 ka), the RSL maximum in Vincennes Bay was in the range of ~30 m (Goodwin, 1993a), considerably higher than most other sectors of the EAIS, i.e. ~10 m in Prydz Bay, MacRobertson Land and Enderby Land (Verleyen et al., 2017; Whitehouse et al., 2012). This difference may suggest a greater amount of ice mass loss in Vincennes Bay compared to other regions, an earlier start to deglaciation (Small et al., 2025), or lower local mantle viscosities (e.g. Lloyd et al., 2020). However, given that the reverse slope and over deepened bathymetry of Vincennes Bay lends itself well to MISI, we interpret the large amount of RSL lowering as having been driven at least partially by rapid retreat across the Bay after onset of deglaciation. This behaviour of rapid retreat across the continental shelf is also observed in Prydz Bay (White et al., 2022) and to a lesser extent in other regions of the EAIS (Kawamata et al., 2020; Suganuma et al., 2022), where the

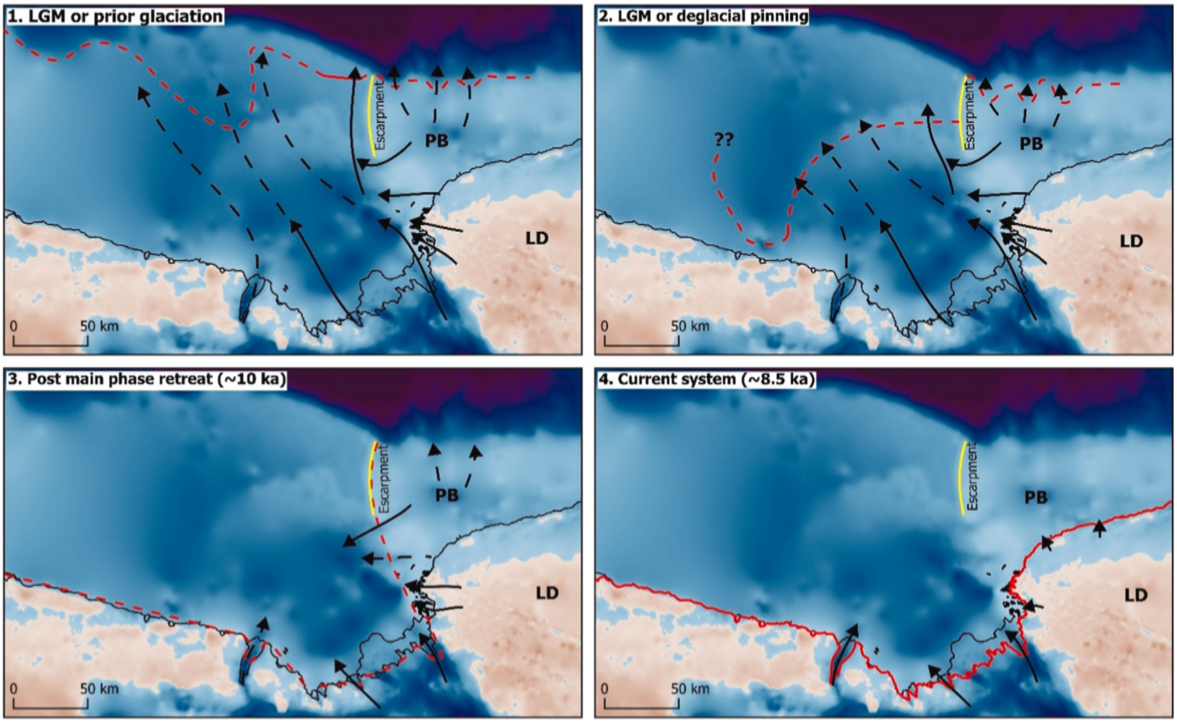

Fig. 9. Phases of grounding line retreat of the regional and periphery ice streams in Vincennes Bay. **Solid black** arrows indicate ice direction constrained by bathymetric features. **Black dashed arrows** are speculative. **Solid red line** is where the grounding of the ice is constrained and a **dashed red line** is our interpretation of a possible grounding line configuration. **Phase 1** is when ice was grounded out to the continental shelf edge at Petersen Bank and directly adjacent the escarpment to the west. How far along the continental shelf it was grounded is not known. **Phase 2** is what we believe the most recent stable glacial configuration, with the grounding line placed on the mid shelf ridge line. **Phase 3** is after the main phase of deglaciation ~10 ka. Ice was still active on Petersen Bank, however the grounding line of the Vanderford, Adams and Underwood Glaciers was near to present. Ice was still present over the shallows flanking Law Dome and the Windmill Islands. **Phase 4** is the final retreat to modern extents ~8.5 ka, noting that there may have been a minor retreat and readvance beyond present in the mid-to-late Holocene. (For interpretation of the references to colour in this figure legend, the reader is referred to the Web version of this article.)

main phase of deglaciation occurred over ~2–4 kyr.

4.2.1. Topographic modulation of retreat

Although changes in accumulation impact the mass balance of glacial systems, those that are marine terminating are particularly susceptible to changes in ocean forcing. Warm water infiltration, such as mCDW, can enhance basal melting (Herraiz-Borreguero et al., 2015; Lanham et al., 2025; Ribeiro et al., 2021; Ye et al., 2024), and increases in sea levels typically have destabilising effects by increasing the proportion of ice that is supported by floatation, thus reducing basal friction (Thomas and Bentley, 1978). Whilst these are well known modes of deglacial forcing, we discuss the influence of local and regional topography on modulating the rate of retreat and stabilisation of the Vincennes Bay glacial system during the main phase of deglaciation post LGM and contrast this with other major glacial systems in the EAIS.

The main phase of deglaciation in Vincennes Bay was largely complete (~10 ka), at a time when Global Mean Sea Level (GSML) and RSL were still increasing (Lambeck et al., 2014; Small et al., 2025). By ~8 ka, local RSL had peaked and begun a phase of RSL fall (Small et al., 2025), which would, if anything, be conducive to grounding line advance. Furthermore, accumulation in the region steadily increased post LGM, a trend seen throughout the EAIS, peaking in the mid-Holocene (Van Ommen et al., 2004). The influence of accumulation is to add positive mass balance to a glacial system and cause advance rather than retreat.

Such an advance is not observed in our data for the over-deepened trenches of the VBIS, however smaller fluctuations are noted later in the Holocene (Section 4.3). We suggest that as the magnitude of any sea-level change is minimal compared to the depth of the Vanderford trench (>2000 m) it likely had little influence on grounding line dynamics and reinforce the idea that marine terminating systems are particularly sensitive to ocean forcing. Given the collapse behaviour inferred during the main phase of post LGM deglaciation in Vincennes Bay, grounding line retreat of the VBIS was likely subject to a MISI effect (Jones et al., 2015; Schoof, 2007). As such the trigger for this collapse was feasibly driven by increased basal melting due to infiltration of mCDW, although local records of oceanic forcing are unavailable.

The western flank of Law Dome retreated over the Windmill Islands between ~9.5 and 8.5 ka (Fig. 8), slowing down after the main phase of deglaciation as it became an increasingly terrestrial margin, pinned on the topographic highs of the Windmill Islands (Appendix B; Figure B.2, Transect C). In contrast to western Law Dome, where retreat was limited after the main phase of deglaciation of the VBIS, the grounded ice centre on Petersen Bank continued a substantive retreat (of 50–75 km). As such the ice on Petersen Bank was either more susceptible to sea level rise, or there was greater access for warm currents to infiltrate the grounding line than at western Law Dome, perhaps as a result of the bank extending to the continental shelf edge where it has a direct connection to the Southern Ocean through deep (>1000 m) troughs. The different retreat patterns evident in Vincennes Bay suggest that bed topography plays a critical role in modulating warm water infiltration, with bed slope and physical pinning points having the greatest influence on how rapidly the ice in this area retreated and where it stabilised.

In other parts of the EAIS basal melt has been highlighted as a likely driver of retreat e.g. Lutzow Holm Bay and the Lambert-Amery system during the post-LGM deglacial (Kawamata et al., 2020; White et al., 2022). However, we know that there is a time transgressive deglaciation history around the EAIS margin following the LGM (Fig. 10). If basal melt was a key control on ice loss, then the bathymetry of the continental shelf would be expected to influence the retreat timing. During the LGM the majority of the EAIS margin was marine terminating, with

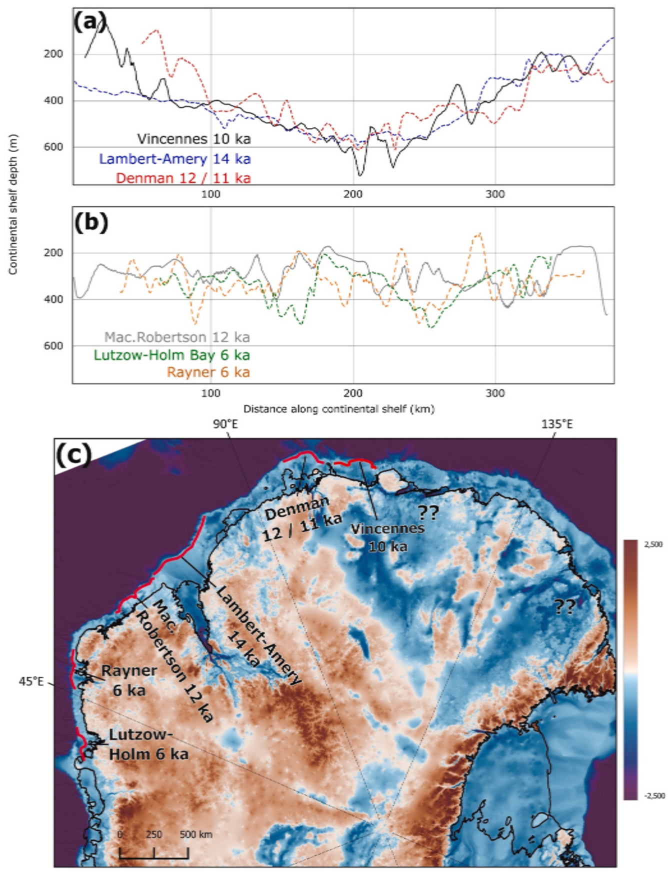

Fig. 10. Continental shelf break geometries of major EAIS basins and timing of retreat. Retreat timing based on when postglacial grounding line reached the modern ice margin (Kawamata et al., 2020; Mackintosh et al., 2011, 2014; White et al., 2022; White and Fink, 2014; Yamane et al., 2011). **Panel (a)** shows three example depth profiles of the continental shelf of glacial systems that have a 'deep' continental shelf break and greater access to warm ocean currents such as mCDW. **Panel (b)** is three examples of 'shallow' shelf systems that are more impeding to warm ocean currents. **Panel (c)** provides an overview of where these depth profiles are (**red lines**). Base layer bed topography utilises data from (Charrassin et al., 2025). **Note (1)** that Mac Robertson Land (~12 ka) retreated early compared to other 'shallow' systems, that we suggest may be due to up-current driven shifts in circulation (Gwyther et al., 2014), being directly west of the Amery Ice Shelf outflow. **Note (2)** that the Denman region retreat timing presented here is based on OSL ages from lake shorelines (Gore et al., 2001) and onset of biogenic sedimentation in lake cores (Berg et al., 2010). (For interpretation of the references to colour in this figure legend, the reader is referred to the Web version of this article.)

transverse continental shelf geometries, such as a reverse slope from the shelf break toward the present grounding line. Thus, the continental shelf break may form a barrier to warmer ocean currents reaching the ice margin. In a scenario of mCDW rising onto the shelf, sectors with deeper continental shelf breaks would be expected to see earlier retreat.

There is a trend toward deeper shelf breaks producing earlier retreats e.g. systems with a wide, deep sill across the shelf break such as Amery, Denman and Vincennes regions retreating between 14 and 10 ka vs shallower systems such as Rayner and Lutzow-Holm Bay retreating by around 6 ka, although the shallowest system of all (Mac. Robertson Land) was also one of the earliest (12 ka) to stabilise (Fig. 10). Given the diachronous retreat timing of these systems, it appears that either oceanic forcing was applied asynchronously around the margin, or other factors (e.g. increased accumulation, or up-current driven shifts in circulation (Gwyther et al., 2014) may have also influenced the onset timing of ice sheet collapse across the continental shelf.

4.3. Mid-to-late Holocene palaeo-environment and ice extents

Regional palaeoclimate records suggest a number of significant, but complex shifts in conditions through the mid to late-Holocene.at 4–3.5 ka (Fig. 11). In the polynya offshore from the Vanderford calving margin, sediment records indicate relatively high biogenic productivity from ~6–3.5 ka and a consistent pattern of biogenic productivity decrease, whilst sea ice associated diatom abundances increase after ~3.5 ka (Harris, 2000; Harris et al., 1997). Whilst the bulk radiocarbon ages used to constrain timing of palaeoenvironmental change in these cores have a considerable level of uncertainty, they are broadly contemporaneous with the changes seen in other proxies discussed below, with the late Holocene trends also consistent with marine cores from other sectors, such as Prydz Bay and Adélie Land (Denis et al., 2010).

A shift also occurs in sediments from the shallow marine environment around Browning Peninsula at this time, with higher biogenic productivity and diatom abundances which has conversely been interpreted as a climatic optimum (Cremer et al., 2003), or as an indication of the isolation of the Windmill Island inlets from the marine environment, due to relative sea level fall (Small et al., 2025). It is notable that the timing is consistent with the period of re-advance of Law Dome based on the minimum age of the reworked shell material (3.4–2.3 cal ka BP) at Ice Cliff 254, with the later exposure ages at the Bailey Peninsula terminal moraine (1.8–1.1 ka) constraining the final retreat to present extents (Fig. 8).

This proposed shift in climatic conditions is coincident with a change in the East Antarctic-wide margin mass balance post 4 ka (Jones et al., 2022; Goodwin, 1998), with Law Dome (DSS and BHC2 cores) and Dome C oxygen isotope records suggesting the atmospheric temperature started warming ~5 ka, peaking at 0.5–0.75 °C above the longer term average at 4–2.5 ka (Goodwin, 1998; Morgan et al., 1997) and in the rate of RSL in the mid to late-Holocene (Small et al., 2025). Such a change in rate would be consistent with an increase in regional ice load, likely due to increased accumulation through the climatic optimum (Goodwin, 1998).

Gradually increasing productivity in the open marine cores from ~6 ka (Harris, 2000; Harris et al., 1997), coupled with increasing atmospheric temperature prior to the climatic optimum ~5 ka (Goodwin, 1998; Morgan et al., 1997) suggest warmer water was present on the continental shelf. It is feasible that the exposure age at Haupt Nunatak (3.7 ka) therefore represents a latter phase of grounding line retreat of the Vanderford Glacier, presenting as a delayed lowering of the ice surface due to hysteresis.

The subsequent pattern of ice margin position and ice load changes and contradictory palaeoclimatic histories recorded in the open marine, shallow marine and lake sediments at ~4-2 ka points to a complex driver of regional palaeoenvironmental change or due to hysteresis in ice response to climate or geophysical forces. A possible explanation for these ice mass changes in the region is a synchronous event controlled by the mid-to-late Holocene climatic optimum and a shift in the relative strength of the Antarctic easterly winds at or post 4 ka.

Stronger easterlies have been modelled to enhance sea ice production in wind driven Antarctic Shelf Front (ASF) dominated ocean circulation regimes such as Vincennes Bay, limiting the amount of warm modified Circumpolar Deep Water (mCDW) incursion toward the grounding line (Lanham et al., 2025) of the Vanderford and other outlet glaciers. This would have the effect of reducing melt at the Vanderford grounding line, producing a regional ice mass gain, as well as decreasing open water diatom abundance and reducing the preservation of organic matter on the sea floor, as observed in sediment cores GC7 and GC8 at this time (Harris, 2000).

A similar climatic optimum is observed in marine inlet and lake sediment records from eastern Prydz Bay (~1500 km east) and the Bunger Hills (~450 km east), the two nearest major terrestrial oases to Vincennes Bay. Marine core samples from Prydz Bay suggest a similar

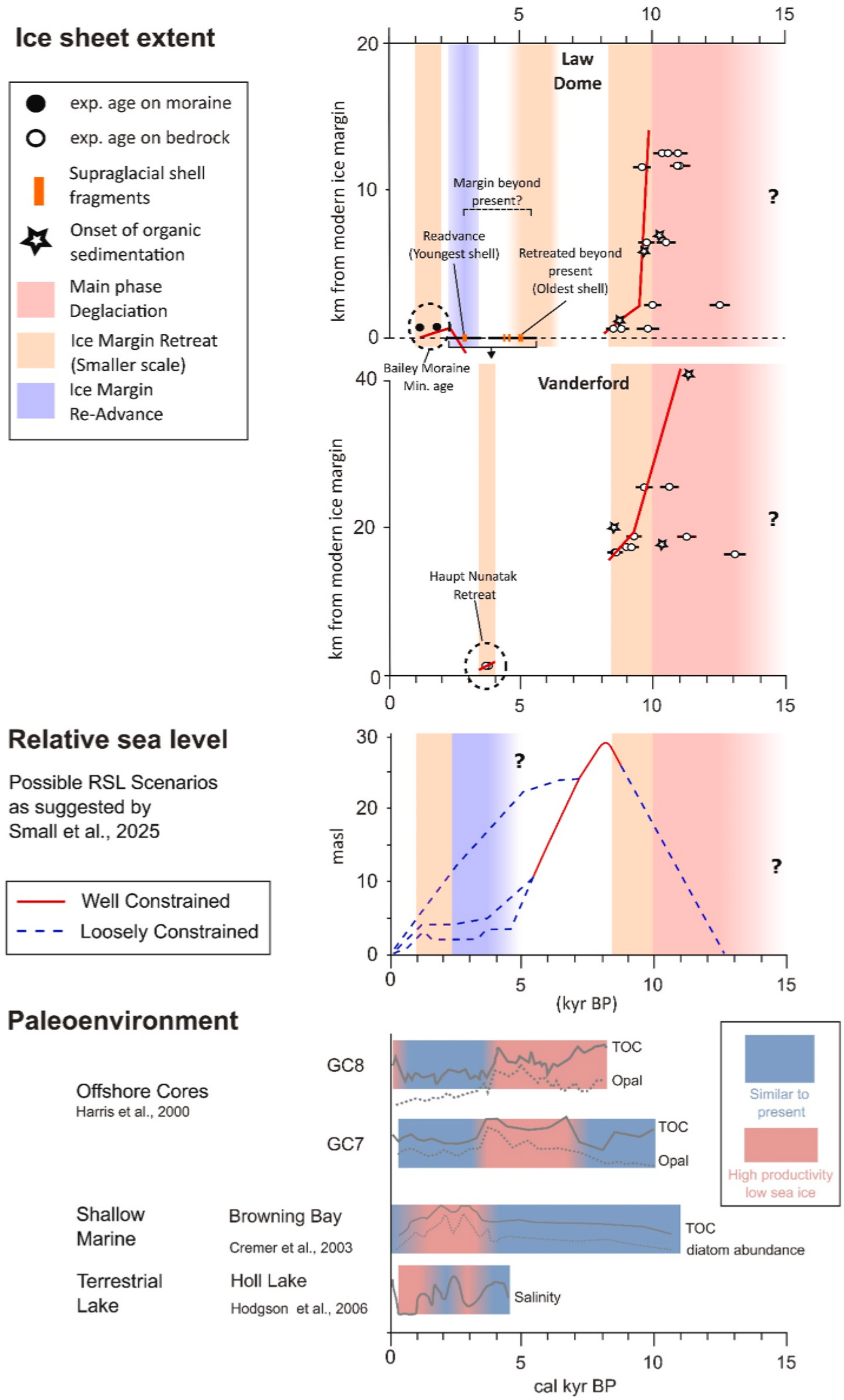

Fig. 11. Comparison of Holocene deglacial timing, relative sea level and palaeoenvironmental records in the Windmill Islands and Snyder Rocks region. **Note (1)** the mid-Holocene change in palaeoenvironmental conditions in the deep marine (Harris, 2000; Harris et al., 1997), shallow marine (Cremer et al., 2003) and lake cores (e.g. Hodgson et al., 2006) at ~4–3.5 ka, which coincides with retreat signatures at Haupt Nunatak. **Note (2)** that RSL is not well constrained through the late Holocene. However, Small et al. (2025) suggest a complex RSL history at this time (dashed blue lines), which is coincident with the timing of change in the palaeoenvironmental proxies and our new evidence of retreat beyond present and subsequent readvance. **Note (3)** that the Bailey moraine samples present a minimum age of retreat, and the youngest reworked ^{14}C age is an estimate of advance. (For interpretation of the references to colour in this figure legend, the reader is referred to the Web version of this article.)

pattern of lesser sea ice from ~7–4.5 ka, with a gradual increase in mixing associated with wind strength. This is followed by increased sea ice and peak wind strength thereafter (Denis et al., 2010). The Vestfold Hills and Rauer Group in Prydz Bay saw an optimum from ~5.5–3.5 ka (White et al., 2022; Berg et al., 2010) suggesting a smaller ice sheet than present and an inferred readvance ~2 ka (White et al., 2022), which is broadly consistent with the Windmill Islands. The ice margin to the east of the Vestfold Hills and Rauer Group is terrestrially grounded, and so less directly influenced by marine drivers of retreat, suggesting atmospheric processes may have played a significant role.

At the Bunger Hills, neighbouring the Denman-Shackleton system, warmer conditions were observed from ~6–2 ka with an optimum from ~4–2 ka (Berg et al., 2020b; Verkulich et al., 2002; Kulbe et al., 2001; Kulbe, 1997). Fluctuations of local glacier extents here have been linked to climate processes, with two or three small advances of the Edisto and Apfel Glaciers through the Holocene suggested by remnant moraines (Augustinus, 2002; Adamson and Colhoun, 1992) and sediment records (Melles et al., 1997). In contrast, sedimentological evidence suggests the regional ice margin to the east of the Bunger Hills has been relatively stable through the mid to late-Holocene (e.g. Doran et al., 2000; Fitzsimons and Colhoun, 1995), since ~5.7 ka (Berg et al., 2020b). In the modern setting, the regional ice to the east is a large blue ice area ablation zone and so it may be expected that any strengthening of the Antarctic Easterlies due to a climatic optimum would, if anything, ablate the ice further. This would therefore make a readvance unlikely at this time and so remains consistent with the underlying hypothesis.

Although the retreat and advance timing among these regions differs slightly, we conclude that climate change rather than geophysical forcing has caused ice margin fluctuations through the mid-to-late Holocene, and that these changes may be consistent with an associated intensification of the large-scale circulation, primarily the Antarctic Easterlies.

5. Conclusions

By interpreting bathymetry, including from recently acquired multibeam data from the continental shelf, we have shown that a regional ice stream was present in Vincennes Bay during the last glacial period (VBIS). Ice was grounded out to the continental shelf adjacent to Petersen Bank, though timing of this phase of glaciation remains uncertain. A large ridge line evident in the mid-shelf region of Vincennes Bay likely represents the pinning point and grounding line of the VBIS during the most recent major ice configuration prior to modern day.

We present new data that constrains the timing of the main phase of deglaciation of the VBIS to near modern extents by ~10 ka, with ice concurrently persistent on Petersen Bank and the Windmill Islands at this time. A retreat history of Western Law Dome through the shallows of the Windmill Islands is observed from ~10 ka to ~8.5 ka, which we suggest represents the approximate timing of deglaciation on Petersen Bank. Onset of deglaciation remains poorly constrained but RSL signatures suggest a large scale or rapid retreat history compared to other regions around the EAIS. This is supported by a reverse sloped bed from the mid shelf ridge to the over deepened glacial troughs afront the modern-day ice streams, ideal for a MISI style retreat.

Continental shelf geometry appears to have an impact on retreat timing of glacial systems in the EAIS, with deeper shelf breaks roughly consistent with earlier retreat timings (Fig. 11). We hypothesise that shallower shelf breaks act to block warm mCDW from entering the shelf. Exceptions to this, such as Mac. Robertson Land (~12 ka), suggest other factors also influence the retreat timing, such as up-current driven shifts in circulation (Gwyther et al., 2014).

We show that climate change forcing has caused ice margin fluctuations through the mid-to-late Holocene, and that these changes may be consistent with an associated intensification of the large-scale circulation, primarily the Antarctic Easterlies and an enhanced ASF blocking mCDW infiltration onto the continental shelf.

CRediT authorship contribution statement

Marcello G. Blaxell: Conceptualisation, Methodology, Formal analysis, Funding acquisition, Investigation, Resources, Writing – original draft, Writing – review & editing, Visualisation, David Small: Investigation, Writing – review & editing, David Fink: Methodology, Resources, Investigation, Writing – review & editing, Réka-H. Fülöp: Methodology, Formal analysis, Resources, Investigation, Validation, Writing – review & editing, Alexandru T. Codilean: Methodology, Formal analysis, Resources, Investigation, Validation, Writing – review & editing, Alexandra Post: Methodology, Investigation, Validation, Writing – review & editing. **Klaus Wilcken:** Methodology, Investigation, Writing – review & editing, Toshiyuki Fujioka: Methodology, Investigation, Writing – review & editing, Sonja Berg: Writing – review & editing, Ian Goodwin: Methodology, Investigation, Sediment sampling for radiocarbon analysis, Writing – review & editing, Steven Phipps: Investigation, Matt Jeromson: Investigation, Writing – review & editing, Duanne A. White: Conceptualisation, Methodology, Investigation, Resources, Supervision, Visualisation, Writing – review & editing.

Declaration of competing interest

The authors declare that they have no known competing financial interests or personal relationships that could have appeared to influence the work reported in this paper.

Acknowledgements

Fieldwork for this study was supported by the Australian Antarctic Division as part of CaDaGIA (AAS4318) and the Australian Research Council (ARC) funded Australian Centre for Excellence in Antarctic Science as part of the preparation for the Denman Terrestrial Campaign (AAS 4630). Sample preparation was undertaken with support from the University of Wollongong and cosmogenic dating at ANSTO through Portals AP11403 and AP12357. M. Blaxell was supported by a University of Canberra HDR scholarship and AINSE PGRA ALNSTU12516. D. Small Acknowledges support from NERC IRF NE/T011963/1. We'd like to thank Tobias Staal, Sue Cook, Anthea Florance, Mic Rolfe and Greg Barras for their support in the field, Krista Simon for laboratory assistance, Mike Bentley for an internal review of the manuscript and Michal Wenderlich and Justy Siwabessy for their work on the RSV Nuyina Voyage 2021-22 multibeam data. S. Phipps was supported under the ARC's Special Research Initiative for the Antarctic Gateway Partnership (Project ID SR140300001).

Appendix A. Supplementary data

Supplementary data to this article can be found online at https://doi.org/10.1016/j.quascirev.2026.109852.

Data availability

A link to the data and/or code is provided as part of this submission.

References

Adamson, D.A., Colhoun, E.A., 1992. Late Quaternary glaciation and deglaciation of the Bunger hills. Antarctica 4, 435–446.

Augustinus, P.C., 2002. Weathering characteristics of the glacial drifts, Bunger hills, East Antarctica. Arct. Antarct. Alp. Res. 34, 65–75. https://doi.org/10.1080/15230430.2002.12003470.

Balco, G., Brown, N., Nichols, K., Venturelli, R. A., Adams, J., Braddock, S., Campbell, S., Goehring, B., Johnson, J. S., Rood, D. H., Wilcken, K., Hall, B., & Woodward, J. (2023). Reversible ice sheet thinning in the Amundsen Sea Embayment during the Late Holocene. *Cryosphere*, *17*(4), 1787–1801. https://doi.org/10.5194/tc-17-1787-2023.

Balco, G., Stone, J.O., Lifton, N.A., Dunai, T.J., 2008. A complete and easily accessible means of calculating surface exposure ages or erosion rates from 10Be and 26Al

measurements. Quat. Geochronol. 3, 174–195. https://doi.org/10.1016/j.quageo.2007.12.001.
Bennett, M.R., Glasser, N.F., 2009. Glacial Geology Ice Sheets and Landforms, second ed., Second. John Wiley & Sons Ltd., West Sussex, UK.
Berg, S., Wagner, B., Cremer, H., Leng, M.J., Melles, M., 2010. Late Quaternary environmental and climate history of Rauer group, East Antarctica. Palaeogeogr. Palaeoclimatol. Palaeoecol. 297, 201–213. https://doi.org/10.1016/j.palaeo.2010.08.002.
Berg, S., Jivcov, S., Kusch, S., Kuhn, G., Wacker, L., Rethemeyer, J., 2020a. Compound-specific radiocarbon analysis of (Sub-)Antarctic coastal marine sediments—potential and challenges for chronologies. Paleoceanogr. Paleoclimatol. 35. https://doi.org/10.1029/2020PA003890.
Berg, S., Melles, M., Gore, D.B., Verkulich, S., Pushina, Z.V., 2020b. Postglacial evolution of marine and lacustrine water bodies in Bunger hills. Antarct. Sci. 32, 107–129. https://doi.org/10.1017/S0954102019000476.
Berkman, P.A., Forman, S.L., 1996. Pre-bomb radiocarbon and the reservoir correction for calcareous marine species in the Southern Ocean. Geophys. Res. Lett. 23, 363–366. https://doi.org/10.1029/96GL00151.
Bird, L.A., Ogarko, V., Ailleres, L., Grose, L., Giraud, J., McCormack, F.S., Gwyther, D.E., Roberts, J.L., Jones, R.S., MacKintosh, A.N., 2025. Gravity-derived Antarctic bathymetry using the Tomofast-x open-source code: a case study of Vincennes Bay. Cryosphere 19 (8), 3355–3380. https://doi.org/10.5194/tc-19-3355-2025.
Blackburn, T., Edwards, G.H., Tulaczyk, S., Scudder, M., Piccione, G., Hallet, B., McLean, N., Zachos, J.C., Cheney, B., Babbe, J.T., 2020. Ice retreat in Wilkes basin of east Antarctica during a warm interglacial. Nature 583, 554–559. https://doi.org/10.1038/s41586-020-2484-5.
Blight, D.F., Oliver, R.L., 1977. The metamorphic geology of the windmill islands, Antarctica: a preliminary account. J. Geol. Soc. Aust. 24, 239–262. https://doi.org/10.1080/00167617708728986.
Borchers, B., Marrero, S., Balco, G., Caffee, M., Goehring, B., Lifton, N., Nishiizumi, K., Phillips, F., Schaefer, J., Stone, J., 2016. Geological calibration of spallation production rates in the CRONUS-earth project. Quat. Geochronol. 31, 188–198. https://doi.org/10.1016/j.quageo.2015.01.009.
Bromwich, D.H., 1988. Snowfall in high southern latitudes. Rev. Geophys. 26, 149–168. https://doi.org/10.1029/RG026i001p00149.
Carson, C., Spinoccia, M., Smith, D., 2016. A High Resolution Bathymetric Grid of the Nearshore Area at Casey Station, Antarctica, Ver. 1. Australian Antarctic Data Centre.
Carson, C., Post, A., Smith, J., Walker, G., Waring, P., Bartley, R., Raymond, B., 2017. The seafloor geomorphology of the Windmill islands, Wilkes land, East Antarctica: evidence of law dome ice margin dynamics. Geomorphology 292, 1–15. https://doi.org/10.1016/j.geomorph.2017.04.031.
Charrassin, R., Millan, R., Rignot, E., Scheinert, M., 2025. Bathymetry of the Antarctic continental shelf and ice shelf cavities from circumpolar gravity anomalies and other data. Sci. Rep. 15. https://doi.org/10.1038/s41598-024-81599-1.
Child, D., Gilbert, E., Mifsud, C., Smith, A., Fink, D., 2000. Sample processing for earth science studies at ANTARES. Nucl. Instrum. Methods Phys. Res. 172, 856–860. https://doi.org/10.1016/S0168-583X(00)00198-1.
Chinn, T.J.H., 1989. Single folds at the margins of dry-based glaciers as indicators of a glacial advance. Ann. Glaciol. 12, 23–30. https://doi.org/10.3189/s0260305500006911.
Clark, C.D., 1993. Mega-scale glacial lineations and cross-cutting ice-flow landforms. Earth Surf. Process. Landf. 18, 1–29. https://doi.org/10.1002/esp.3290180102.
Codilean, A.T., Fülöp, R.H., Wilcken, K.M., Koutamanis, D.S., Fink, D., Fifield, L.K., Wong, H., Enge, T.G., Vardanega, C., Rowling, B., 2023. Cosmogenic 10Be and 26Al sample preparation at the University of Wollongong. Nucl. Instrum. Methods Phys. Res. B 535, 61–73. https://doi.org/10.1016/j.nimb.2022.12.003.
Commonwealth of Australia, 2022. RSV Nuyina voyage 2 2021-22 voyage data, Southern Ocean, Antarctica. https://doi.org/10.26179/ZZ6J-E834.
Commonwealth of Australia, 2024. RSV Nuyina voyage data 2023-24 V2, ver. 1. https://doi.org/10.26179/n6cj-qd63.
Cook, C.P., Van De Flierdt, T., Williams, T., Hemming, S.R., Iwai, M., Kobayashi, M., Jimenez-Espejo, F.J., Escutia, C., González, J.J., Khim, B.K., McKay, R.M., Passchier, S., Bohaty, S.M., Riesselman, C.R., Tauxe, L., Sugisaki, S., Galindo, A.L., Patterson, M.O., Sangiorgi, F., Pierce, E.L., Brinkhuis, H., Klaus, A., Fehr, A., Bendle, J.A.P., Bijl, P.K., Carr, S.A., Dunbar, R.B., Flores, J.A., Hayden, T.G., Katsuki, K., Kong, G.S., Nakai, M., Olney, M.P., Pekar, S.F., Pross, J., Röhl, U., Sakai, T., Shrivastava, P.K., Stickley, C.E., Tuo, S., Welsh, K., Yamane, M., 2013. Dynamic behaviour of the East Antarctic ice sheet during Pliocene warmth. Nat. Geosci. 6, 765–769. https://doi.org/10.1038/ngeo1889.
Cremer, H., Gore, D., Melles, M., Roberts, D., 2003. Palaeoclimatic significance of late Quaternary diatom assemblages from southern Windmill Islands , East Antarctica. Palaeogeogr. Palaeoclimatol. Palaeoecol. 195, 261–280. https://doi.org/10.1016/S0031-0182(03)00361-4.
Davison, B.J., Hogg, A.E., Gourmelen, N., Jakob, L., Wuite, J., Nagler, T., Greene, C.A., Andreasen, J., Engdahl, M.E., 2023. Annual mass budget of Antarctic ice shelves from 1997 to 2021. Sci. Adv. 9. https://doi.org/10.1126/sciadv.adi0186.
DeConto, R.M., Pollard, D., Alley, R.B., Velicogna, I., Gasson, E., Gomez, N., Sadai, S., Condron, A., Gilford, D.M., Ashe, E.L., Kopp, R.E., Li, D., Dutton, A., 2021. The paris climate agreement and future sea-level rise from Antarctica. Nature 593, 83–89. https://doi.org/10.1038/s41586-021-03427-0.
Denis, D., Crosta, X., Barbara, L., Massé, G., Renssen, H., Ther, O., Giraudeau, J., 2010. Sea ice and wind variability during the Holocene in East Antarctica: insight on middle-high latitude coupling. Quat. Sci. Rev. 29, 3709–3719. https://doi.org/10.1016/j.quascirev.2010.08.007.
Divola, C., Simms, A.R., Sremba, A., Baker, C.S., Friedlaender, A., Southon, J., 2024. Constraining the radiocarbon reservoir age for the Southern Ocean using whale bones salvaged from early 20th century whaling stations. Quat. Sci. Rev. 336. https://doi.org/10.1016/j.quascirev.2024.108756.
Doran, P.T., Wharton, R.A., Lyons, W.B., Marais, D.J.D., Andersen, D.T., 2000. Sedimentology and geochemistry of a perennially ice-covered epishelf lake in Bunger hills Oasis, East Antarctica. Antarct. Sci. 12 (2), 131–140. https://doi.org/10.1017/S0954102000000171.
Dorschel, B., Hehemann, L., Viquerat, S., Warnke, F., Dreutter, S., Schulze Tenberge, Y., Accettella, D., An, L., Barrios, F., Bazhenova, E.A., Black, J., Bohoyo, F., Davey, C., de Santis, L., Escutia Dotti, C., Frémand, A.C., Fretwell, P.T., Gales, J.A., Gao, J., Gasperini, L., Greenbaum, J.S., Henderson Jencks, J., Hogan, K.A., Hong, J.K., Jakobsson, M., Jensen, L., Kool, J., Larin, S., Larter, R.D., Leitchenkov, G.L., Loubrieu, B., Mackay, K., Mayer, L., Millan, R., Morlighem, M., Navidad, F., Nitsche, F.-O., Nogi, Y., Pertuisot, C., Post, A.L., Pritchard, H.D., Purser, A., Rebesco, M., Rignot, E., Roberts, J.L., Rovere, M., Ryzhov, I., Sauli, C., Schmitt, T., Silvano, A., Smith, J.E., Snaith, H., Tate, A.J., Tinto, K., Vandenbossche, P., Weatherall, P., Wintersteller, P., Yang, C., Zhang, T., Arndt, J.E., 2022. The international bathymetric chart of the Southern Ocean version 2 (IBCSO v2). https://doi.org/10.1594/PANGAEA.937574.
Dupont, T.K., Alley, R.B., 2005. Assessment of the importance of ice-shelf buttressing to ice-sheet flow. Geophys. Res. Lett. 32, 1–4. https://doi.org/10.1029/2004GL022024.
Eayrs, C., Li, X., Raphael, M.N., Holland, D.M., 2021. Rapid decline in Antarctic sea ice in recent years hints at future change. Nat. Geosci. https://doi.org/10.1038/s41561-021-00768-3.
Edwards, T.L., Nowicki, S., Marzeion, B., Hock, R., Goelzer, H., Seroussi, H., Jourdain, N. C., Slater, D.A., Turner, F.E., Smith, C.J., McKenna, C.M., Simon, E., Abe-Ouchi, A., Gregory, J.M., Larour, E., Lipscomb, W.H., Payne, A.J., Shepherd, A., Agosta, C., Alexander, P., Albrecht, T., Anderson, B., Asay-Davis, X., Aschwanden, A., Barthel, A., Bliss, A., Calov, R., Chambers, C., Champollion, N., Choi, Y., Cullather, R., Cuzzone, J., Dumas, C., Felikson, D., Fettweis, X., Fujita, K., Galton-Fenzi, B.K., Gladstone, R., Golledge, N.R., Greve, R., Hattermann, T., Hoffman, M.J., Humbert, A., Huss, M., Huybrechts, P., Immerzeel, W., Kleiner, T., Kraaijenbrink, P., Le clec'h, S., Lee, V., Leguy, G.R., Little, C.M., Lowry, D.P., Malles, J.H., Martin, D.F., Maussion, F., Morlighem, M., O'Neill, J.F., Nias, I., Pattyn, F., Pelle, T., Price, S.F., Quiquet, A., Radić, V., Reese, R., Rounce, D.R., Rückamp, M., Sakai, A., Shafer, C., Schlegel, N.J., Shannon, S., Smith, R.S., Straneo, F., Sun, S., Tarasov, L., Trusel, L.D., Van Breedam, J., van de Wal, R., van den Broeke, M., Winkelmann, R., Zekollari, H., Zhao, C., Zhang, T., Zwinger, T., 2021. Projected land ice contributions to twenty-first-century sea level rise. Nature 593, 74–82. https://doi.org/10.1038/s41586-021-03302-y.
Emslie, S.D., Woehler, E.J., 2005. A 9000-year record of Adélie penguin occupation and diet in the Windmill islands. East Antarctica 17, 57–66. https://doi.org/10.1017/S0954102005002427.
Fink, D., Smith, A., 2007. An inter-comparison of 10Be and 26Al AMS reference standards and the 10Be half-life. Nucl. Instrum. Methods Phys. Res. B 259, 600–609. https://doi.org/10.1016/j.nimb.2007.01.299.
Fitzsimons, S.J., Colhoun, E.A., 1995. Form, structure and stability of the margin of the Antarctic ice sheet, Vestfold hills and Bunger hills, East Antarctica. Antarct. Sci 7 (2), 171–179. https://doi.org/10.1017/S095410209500023X.
Flament, T., Rémy, F., 2012. Dynamic thinning of Antarctic glaciers from along-track repeat radar altimetry. J. Glaciol. 58, 830–840. https://doi.org/10.3189/2012jog11j118.
Foerste, C., Bruinsma, SeanL., Abrykosov, O., Lemoine, J.-M., Marty, J.C., Flechtner, F., Balmino, G., Barthelmes, F., Biancale, R., 2014. EIGEN-6C4 the Latest Combined Global Gravity Field Model Including GOCE Data up to Degree and Order 2190 of GFZ Potsdam and GRGS Toulouse. https://doi.org/10.5880/icgem.2015.1.
Fretwell, P., Pritchard, H.D., Vaughan, D.G., Bamber, J.L., Barrand, N.E., Bell, R., Bianchi, C., Bingham, R.G., Blankenship, D.D., Casassa, G., Catania, G., Callens, D., Conway, H., Cook, A.J., Corr, H.F.J., Damaske, D., Damm, V., Ferraccioli, F., Forsberg, R., Fujita, S., Gim, Y., Gogineni, P., Griggs, J.A., Hindmarsh, R.C.A., Holmlund, P., Holt, J.W., Jacobel, R.W., Jenkins, A., Jokat, W., Jordan, T., King, E. C., Kohler, J., Krabill, W., Riger-Kusk, M., Langley, K.A., Leitchenkov, G., Leuschen, C., Luyendyk, B.P., Matsuoka, K., Mouginot, J., Nitsche, F.O., Nogi, Y., Nost, O.A., Popov, S.V., Rignot, E., Rippin, D.M., Rivera, A., Roberts, J., Ross, N., Siegert, M.J., Smith, A.M., Steinhage, D., Studinger, M., Sun, B., Tinto, B.K., Welch, B.C., Wilson, D., Young, D.A., Xiangbin, C., Zirizzotti, A., 2013. Bedmap2: improved ice bed, surface and thickness datasets for Antarctica. Cryosphere 7, 375–393. https://doi.org/10.5194/tc-7-375-2013.
Golledge, N.R., Kowalewski, D.E., Naish, T.R., Levy, R.H., Fogwill, C.J., Gasson, E.G.W., 2015. The multi-millennial Antarctic commitment to future sea-level rise. Nature 526, 421–425. https://doi.org/10.1038/nature15706.
Goodwin, I., 1993a. Holocene deglaciation, sea-level change, and the emergence of the windmill islands, Budd Coast, Antarctica. Quat Res 40, 55–69. https://doi.org/10.1006/qres.1993.1057.
Goodwin, I., 1993b. Basal ice accretion and debris entrainment at law dome margin. J. Glaciol. 39, 157–166. https://doi.org/10.3189/S002214300001580X.
Goodwin, I., 1996. A mid to late Holocene readvance of the law dome ice margin, Budd Coast, East Antarctica. Antarct. Sci. 8, 395–406. https://doi.org/10.1017/s0954102096000570.
Goodwin, I.D., 1998. Did changes in Antarctic ice volume influence late Holocene sea-level lowering? Quat. Sci. Rev. 17, 319–332. https://doi.org/10.1016/S0277-3791(97)00051-6.
Goodwin, I.D., Roberts, J.L., Etheridge, D.M., Hellstrom, J., Moy, A.D., Ribo, M., Smith, A.M., 2018. Modern to glacial age subglacial meltwater drainage at law

dome, coastal East Antarctica from topography, sediments and jökulhlaup observations. Geol Soc Spec Publ 461, 215–230. https://doi.org/10.1144/SP461.16.
Gore, D.B., Leishman, M.R., 2020. Salt, sediments and weathering environments in Bunger hills. Antarct. Sci. 32, 138–152. https://doi.org/10.1017/S0954102020000073.
Gore, D.B., Rhodes, E.J., Augustinus, P.C., Leishman, M.R., Colhoun, E.A., Rees-Jones, J., 2001. Bunger hills, East Antarctica: ice free at the last glacial maximum. Geology 29, 1103–1106. https://doi.org/10.1130/0091-7613.
Gudmundsson, G.H., 2013. Ice-shelf buttressing and the stability of marine ice sheets. Cryosphere 7, 647–655. https://doi.org/10.5194/tc-7-647-2013.
Gwyther, D.E., Galton-Fenzi, B.K., Hunter, J.R., Roberts, J.L., 2014. Simulated melt rates for the Totten and Dalton ice shelves. Ocean Sci. 10, 267–279. https://doi.org/10.5194/os-10-267-2014.
Harris, P.T., 2000. Sedimentological Signatures of sub-ice-shelf Circulation: an Example from Vincennes Bay, East Antarctica, 133. Papers and Proceedings of the Royal Society of Tasmania. https://doi.org/10.26749/rstpp.133.2.57.
Harris, P.T., Domack, E., Goodwin, I., Quilty, P., 1997. Glacimarine siliciclastic muds from vincennes Bay, East Antarctica; preliminary results of an exploratory cruise in 1997 plastic pollution in the marine environment view project global seafloor geomorphic features map view project. Terra Antarctica 4, 11–22.
Heaton, T.J., Köhler, P., Butzin, M., Bard, E., Reimer, R.W., Austin, W.E.N., Bronk Ramsey, C., Grootes, P.M., Hughen, K.A., Kromer, B., Reimer, P.J., Adkins, J., Burke, A., Cook, M.S., Olsen, J., Skinner, L.C., 2020. Marine20 - the marine radiocarbon age calibration curve (0-55,000 cal BP). Radiocarbon 62, 779–820. https://doi.org/10.1017/RDC.2020.68.
Helm, V., Humbert, A., Miller, H., 2014. Elevation and elevation change of Greenland and Antarctica derived from CryoSat-2. Cryosphere 8, 1539–1559. https://doi.org/10.5194/tc-8-1539-2014.
Herraiz-Borreguero, L., Coleman, R., Allison, I., Rintoul, S.R., Craven, M., Williams, G.D., 2015. Circulation of modified circumpolar deep water and basal melt beneath the Amery Ice Shelf, East Antarctica. J. Geophys. Res. C Oceans 120, 3098–3112. https://doi.org/10.1002/2015JC010697.
Hodgson, D.A., Roberts, D., McMinn, A., Verleyen, E., Terry, B., Corbett, C., Vyverman, W., 2006. Recent rapid salinity rise in three East Antarctic lakes. J. Paleolimnol. 36, 385–406. https://doi.org/10.1007/s10933-006-9010-0.
Howat, I., Porter, C., Noh, M.-J., Husby, E., Khuvis, S., Danish, E., Tomko, K., Gardiner, J., Negrete, A., Yadav, B., Klassen, J., Kelleher, C., Cloutier, M., Bakker, J., Enos, J., Arnold, G., Bauer, G., Morin, P., Foundation, N.S., NASA, 2022. The reference elevation model of Antarctica - mosaics, Version 2. https://doi.org/10.7910/DVN/EBW8UC.
Jamieson, S.S.R., Stokes, C.R., Livingstone, S.J., Vieli, A., Cofaigh, C., Hillenbrand, C.D., Spagnolo, M., 2016. Subglacial processes on an Antarctic ice stream bed. 2: can modelled ice dynamics explain the morphology of mega-scale glacial lineations? J. Glaciol. 62, 285–298. https://doi.org/10.1017/jog.2016.19.
Johnson, J.S., Venturelli, R.A., Balco, G., Allen, C.S., Braddock, S., Campbell, S., Goehring, B.M., Hall, B.L., Neff, P.D., Nichols, K.A., Rood, D.H., Thomas, E.R., Woodward, J., 2022. Review article: existing and potential evidence for Holocene grounding line retreat and readvance in Antarctica. Cryosphere 16, 1543–1562. https://doi.org/10.5194/tc-16-1543-2022.
Jones, R.S., Mackintosh, A.N., Norton, K.P., Golledge, N.R., Fogwill, C.J., Kubik, P.W., Christl, M., Greenwood, S.L., 2015. Rapid Holocene thinning of an East Antarctic outlet glacier driven by marine ice sheet instability. Nat. Commun. 6, 1–9. https://doi.org/10.1038/ncomms9910.
Jones, R.S., Johnson, J.S., Lin, Y., Mackintosh, A.N., Sefton, J.P., Smith, J.A., Thomas, E. R., Whitehouse, P.L., 2022. Stability of the Antarctic Ice sheet during the pre-industrial Holocene. Nat. Rev. Earth Environ. 3, 500–515. https://doi.org/10.1038/s43017-022-00309-5.
Jong, L.M., Plummer, C.T., Roberts, J.L., Moy, A.D., Curran, M.A.J., Vance, T.R., Pedro, J.B., Long, C.A., Nation, M., Mayewski, P.A., Van Ommen, T.D., 2022. 2000 years of annual ice core data from law dome, East Antarctica. Earth Syst. Sci. Data 14, 3313–3328. https://doi.org/10.5194/essd-14-3313-2022.
Kawamata, M., Suganuma, Y., Doi, K., Misawa, K., Hirabayashi, M., Hattori, A., Sawagaki, T., 2020. Abrupt Holocene ice-sheet thinning along the southern Soya Coast, Lützow-Holm Bay, East Antarctica, revealed by glacial geomorphology and surface exposure dating. Quat. Sci. Rev. 247. https://doi.org/10.1016/j.quascirev.2020.106540.
Kiernan, K., Gore, D.B., Fink, D., White, D.A., McConnell, A., Sigurdsson, I.A., 2009. Deglaciation and weathering of larsemann hills, East Antarctica. Antarct. Sci. 21, 373–382. https://doi.org/10.1017/S0954102009002028.
King, E.C., Hindmarsh, R.C.A., Stokes, C.R., 2009. Formation of mega-scale glacial lineations observed beneath a West Antarctic ice stream. Nat. Geosci. 2, 585–588. https://doi.org/10.1038/ngeo581.
Kirkup, H., Melles, M., Gore, D.B., 2002. Late Quaternary environment of southern Windmill islands, East Antarctica. Antarct. Sci. 14, 385–394. https://doi.org/10.1017/S0954102002000202.
Kohl, C.P., Nishiizumi, K., 1992. Scientific comment chemical isolation of quartz for measurement of in-situ-produced cosmogenic nuclides. Geochimica et Cosmochimica Acla 56, 3583–3587. https://doi.org/10.1016/0016-7037(92)90401-4.
Kulbe, T., 1997. The late quaternary climatic and environmental history of Bunger Oasis, East Antarctica. Rep. Polar Res. 254.
Kulbe, T., Melles, M., Verkulich, S.R., Pushina, Z.V., 2001. East antarctic climate and environmental variability over the last 9400 years inferred from marine sediments of the bunger oasis. Arct. Antarct. Alp. Res 33, 223–230. https://doi.org/10.1080/15230430.2001.12003425.
Lambeck, K., Rouby, H., Purcell, A., Sun, Y., Sambridge, M., 2014. Sea Level and Global Ice Volumes from the Last Glacial Maximum to the Holocene, 111. Proceedings of the National Academy of Sciences, pp. 15296–15303. https://doi.org/10.1073/pnas.1411762111.
Lanham, J., Mazloff, M., Naveira Garabato, A.C., Siegert, M., Mashayek, A., 2025. Seasonal regimes of warm circumpolar deep water intrusion toward Antarctic ice shelves. Commun. Earth Environ. 6. https://doi.org/10.1038/s43247-025-02091-w.
Lifton, N., Sato, T., Dunai, T.J., 2014. Scaling in situ cosmogenic nuclide production rates using analytical approximations to atmospheric cosmic-ray fluxes. Earth Planet Sci. Lett. 386, 149–160. https://doi.org/10.1016/j.epsl.2013.10.052.
Livingstone, S.J., Stokes, C.R., Cofaigh, C., Hillenbrand, C.D., Vieli, A., Jamieson, S.S.R., Spagnolo, M., Dowdeswell, J.A., 2016. Subglacial processes on an Antarctic ice stream bed. 1: sediment transport and bedform genesis inferred from marine geophysical data. J. Glaciol. 62, 270–284. https://doi.org/10.1017/jog.2016.18.
Lloyd, A.J., Wiens, D.A., Zhu, H., Tromp, J., Nyblade, A.A., Aster, R.C., Hansen, S.E., Dalziel, I.W.D., Wilson, T.J., Ivins, E.R., O'Donnell, J.P., 2020. Seismic structure of the antarctic upper mantle imaged with adjoint tomography. J. Geophys. Res. Solid Earth 125. https://doi.org/10.1029/2019JB017823.
Mackintosh, A., Golledge, N., Domack, E., Dunbar, R., Leventer, A., White, D., Pollard, D., DeConto, R., Fink, D., Zwartz, D., Gore, D., Lavoie, C., 2011. Retreat of the East Antarctic ice sheet during the last glacial termination. Nat. Geosci. 4, 195–202. https://doi.org/10.1038/ngeo1061.
Mackintosh, A., Verleyen, E., O'Brien, P.E., White, D.A., Jones, R.S., McKay, R., Dunbar, R., Gore, D.B., Fink, D., Post, A.L., Miura, H., Leventer, A., Goodwin, I., Hodgson, D.A., Lilly, K., Crosta, X., Golledge, N.R., Wagner, B., Berg, S., van Ommen, T., Zwartz, D., Roberts, S.J., Vyverman, W., Masse, G., 2014. Retreat history of the East Antarctic Ice sheet since the last glacial maximum. Quat. Sci. Rev. 100, 10–30. https://doi.org/10.1016/j.quascirev.2013.07.024.
Matthews, J.A., Shakesby, R.A., 1984. The status of the "Little Ice Age" in southern Norway: relative-age dating of neoglacial moraines with schmidt hammer and lichenometry. Boreas 13, 333–346. https://doi.org/10.1111/j.1502-3885.1984.tb01128.x.
McCormack, F.S., Roberts, J.L., Kulessa, B., Aitken, A., Dow, C.F., Bird, L., Galton-Fenzi, B.K., Hochmuth, K., Jones, R.S., MacKintosh, A.N., McArthur, K., 2023. Assessing the potential for ice flow piracy between the Totten and Vanderford glaciers, East Antarctica. Cryosphere 17, 4549–4569. https://doi.org/10.5194/tc-17-4549-2023.
McMahon, C.R., Hindell, M.A., Charrassin, J.B., Coleman, R., Guinet, C., Harcourt, R., Labrousse, S., Raymond, B., Sumner, M., Ribeiro, N., 2023. Southern Ocean pinnipeds provide bathymetric insights on the East Antarctic continental shelf. Commun. Earth Environ. 4. https://doi.org/10.1038/s43247-023-00928-w.
Melles, M., Kulbe, T., Verkulich, S.R., Pushina, Z.V., Hubberten, H.-W., 1997. Late Pleistocene and Holocene environmental history of Bunger hills, East Antarctica, as revealed by fresh-water and epishelf Lake sediments. In: Ricci, C.A. (Ed.), The Antarctic Region: Geological Evolution and Processes. Terra Antarctica Publications, Sienna, Italy, pp. 809–820.
Morgan, V.I., Wookey, C.W., Li, J., van Ommen, T.D., Skinner, W., Fitzpatrick, M.F., 1997. Site information and initial results from deep ice drilling on Law Dome, Antarctica. J. Glaciol. 43, 3–10. https://doi.org/10.3189/s0022143000002768.
Moriwaki, K., Iwata, S., Matsuoka, N., Hasegawa, H., Hirakawa, K., 1994. Weathering stage as a relative age of till in the central Sør-Rondane. In: Proceedings of the NIPR Symposium on Antarctic Geoscience, pp. 156–161.
Morlighem, M., Rignot, E., Binder, T., Blankenship, D., Drews, R., Eagles, G., Eisen, O., Ferraccioli, F., Forsberg, R., Fretwell, P., Goel, V., Greenbaum, J.S., Gudmundsson, H., Guo, J., Helm, V., Hofstede, C., Howat, I., Humbert, A., Jokat, W., Karlsson, N.B., Lee, W.S., Matsuoka, K., Millan, R., Mouginot, J., Paden, J., Pattyn, F., Roberts, J., Rosier, S., Ruppel, A., Seroussi, H., Smith, E.C., Steinhage, D., Sun, B., Broeke, M.R. van den, Ommen, T.D. van, Wessem, M. van, Young, D.A., 2020. Deep glacial troughs and stabilizing ridges unveiled beneath the margins of the Antarctic ice sheet. Nat. Geosci. 13, 132–137. https://doi.org/10.1038/s41561-019-0510-8.
Mouginot, J., Scheuchl, B., Rignot, E., 2017. MEaSUREs antarctic boundaries for IPY 2007-2009 from satellite radar, version 2. MEaSUREs antarctic grounding line from differential satellite radar interferometry. https://doi.org/10.5067/AXE4121732AD.
Nishiizumi, K., Imamura, M., Caffee, M.W., Southon, J.R., Finkel, R.C., McAninch, J., 2007. Absolute calibration of 10Be AMS standards. Nucl. Instrum. Methods Phys. Res. B 258, 403–413. https://doi.org/10.1016/j.nimb.2007.01.297.
O'Brien, P.E., De Santis, L., Harris, P.T., Domack, E., Quilty, P.G., 1999. Ice shelf grounding zone features of western Prydz Bay, Antarctica: sedimentary processes from seismic and sidescan images. Antarct. Sci. 11, 78–91. https://doi.org/10.1017/S0954102099000115.
O'Brien, P.E., Beaman, R., De Santis, L., Domack, E.W., Escutia, C., Harris, P.T., Leventer, A., McMullen, K., Post, A., Quilty, P.G., Shevenell, A.E., Batchelor, C.L., 2016. Submarine glacial landforms on the cold East Antarctic margin. Geological Society Memoir 46, 501–508. https://doi.org/10.1144/M46.172.
Okuno, J., Hattori, A., Doi, K., Aoyama, Y., Fukuda, Y., 2025. Mid Holocene rapid thinning and rethickening of the East Antarctic ice sheet suggested by glacial isostatic adjustment. Scientific Reports 15 (1). https://doi.org/10.1038/s41598-025-24176-4.
Paul, E., Stuwe, K., Teasdale, U.J., Worley, B., 1995. Structural and metamorphic geology of the Windmill islands, east Antarctica: field evidence for repeated tectonothermal activity. Aust. J. Earth Sci. 42, 453–469. https://doi.org/10.1080/08120099508728216.
Pelle, T., Morlighem, M., McCormack, F.S., 2020. Aurora basin, the weak underbelly of East Antarctica. Geophys. Res. Lett. 47. https://doi.org/10.1029/2019GL086821.

Pfitzner, M.L., 1980. The Wilkes Ice Cap Project, 1966/M.L. Pfitzner. Australian Government Publishing Service, Canberra.
Picton, H.J., Stokes, C.R., Jamieson, S.S.R., Floricioiu, D., Krieger, L., 2023. Extensive and anomalous grounding line retreat at vanderford glacier, Vincennes Bay, Wilkes Land, East Antarctica. Cryosphere 17, 3593–3616. https://doi.org/10.5194/tc-17-3593-2023.
Pollard, D., Deconto, R., 2016. Contribution of Antarctica to past and future sea-level rise. Nature 531, 591–597. https://doi.org/10.1038/nature17145.
Pritchard, H.D., Arthern, R.J., Vaughan, D.G., Edwards, L.A., 2009. Extensive dynamic thinning on the margins of the Greenland and Antarctic ice sheets. Nature 461, 971–975. https://doi.org/10.1038/nature08471.
Pritchard, H., Fretwell, P., Fremand, A., Bodart, J., Kirkham, J., Aitken, A., Bamber, J., Bell, R., Bianchi, C., Bingham, R., Blankenship, D., Casassa, G., Catania, G., Christianson, K., Conway, H., Corr, H., Cui, X., Damaske, D., Damn, V., Drews, R., Eagles, G., Eisen, O., Eisermann, H., Ferraccioli, F., Forsberg, R., Franke, S., Fujita, S., Gim, Y., Goel, V., Prasad Gogineni, S., Greenbaum, J., Hills, B., Hindmarsh, R., Holmlund, P., Holschuh, N., Holt, J., Humbert, A., Jacobel, R., Jansen, D., Jenkins, A., Jokat, W., Jordan, T., King, E., Kohler, J., Krabill, W., Langley, K., Lee, J., Leitchenkov, G., Leuschen, C., Luyendyk, B., MacGregor, J., MacKie, E., Matsuoka, K., Morlighem, M., Mouginot, J., Nitsche, F., Nogi, Y., Nost, O., Paden, J., Pattyn, F., Popov, S., Kusk-Gillespie, M., Rignot, E., Rippin, D., Rivera, A., Ross, N., Ruppel, A., Schroeder, D., Siegert, M., Smith, A., Steinhage, D., Studinger, M., Sun, B., Tabacco, I., Tinto, K., Urbini, S., Vaughan, D., Welch, B., Wilson, D., Young, D., Zirizzotti, A., 2024. BEDMAP3 - Ice thickness, bed and surface elevation for Antarctica - gridding products, Version 1.0. https://doi.org/10.5285/2d0e4791-8e20-46a3-80e4-f5f6716025d2.
Pritchard, H.D., Fretwell, P.T., Fremand, A.C., Bodart, J.A., Kirkham, J.D., Aitken, A., Bamber, J., Bell, R., Bianchi, C., Bingham, R.G., Blankenship, D.D., Casassa, G., Christianson, K., Conway, H., Corr, H.F.J., Cui, X., Damaske, D., Damm, V., Dorschel, B., Drews, R., Eagles, G., Eisen, O., Eisermann, H., Ferraccioli, F., Field, E., Forsberg, R., Franke, S., Goel, V., Gogineni, S.P., Greenbaum, J., Hills, B., Hindmarsh, R.C.A., Hoffman, A.O., Holschuh, N., Holt, J.W., Humbert, A., Jacobel, R.W., Jansen, D., Jenkins, A., Jokat, W., Jong, L., Jordan, T.A., King, E.C., Kohler, J., Krabill, W., Maton, J., Gillespie, M.K., Langley, K., Lee, J., Leitchenkov, G., Leuschen, C., Luyendyk, B., MacGregor, J.A., MacKie, E., Moholdt, G., Matsuoka, K., Morlighem, M., Mouginot, J., Nitsche, F.O., Nost, O.A., Paden, J., Pattyn, F., Popov, S., Rignot, E., Rippin, D.M., Rivera, A., Roberts, J.L., Ross, N., Ruppel, A., Schroeder, D.M., Siegert, M.J., Smith, A.M., Steinhage, D., Studinger, M., Sun, B., Tabacco, I., Tinto, K.J., Urbini, S., Vaughan, D.G., Wilson, D. S., Young, D.A., Zirizzotti, A., 2025. Bedmap3 updated ice bed, surface and thickness gridded datasets for Antarctica. Sci. Data 12, 414. https://doi.org/10.1038/s41597-025-04672-y.
Purich, A., Doddridge, E.W., 2023. Record low Antarctic sea ice coverage indicates a new sea ice state. Commun. Earth Environ. 4. https://doi.org/10.1038/s43247-023-00961-9.
Ribeiro, N., Herraiz-Borreguero, L., Rintoul, S.R., McMahon, C.R., Hindell, M., Harcourt, R., Williams, G., 2021. Warm modified circumpolar deep water intrusions drive ice shelf melt and inhibit dense shelf water formation in vincennes Bay, East Antarctica. J. Geophys. Res., Oceans 126. https://doi.org/10.1029/2020JC016998.
Rignot, E., Casassa, G., Gogineni, P., Krabill, W., Rivera, A., Thomas, R., 2004. Accelerated ice discharge from the Antarctic peninsula following the collapse of Larsen B ice shelf. Geophys. Res. Lett. 31, 2–5. https://doi.org/10.1029/2004GL020697.
Rignot, E., Mouginot, J., Scheuchl, B., Van Den Broeke, M., Van Wessem, M.J., Morlighem, M., 2019. Four decades of Antarctic ice sheet mass balance from 1979–2017. Proc. Natl. Acad. Sci. U. S. A. 116, 1095–1103. https://doi.org/10.1073/pnas.1812883116.
Roberts, D., McMinn, A., Cremer, H., Gore, D.B., Melles, M., 2004. The Holocene evolution and palaeosalinity history of beall Lake, Windmill Islands (East Antarctica) using an expanded diatom-based weighted averaging model. Palaeogeogr. Palaeoclimatol. Palaeoecol. 208, 121–140. https://doi.org/10.1016/j.palaeo.2004.02.032.
Rott, H., Skvarca, P., Nagler, T., 1996. Rapid collapse of the Northern larsen ice shelf, Antacrtica. Science 271, 788–792. https://doi.org/10.1126/science.271.5250.7.
Sadatzki, H., Opdyke, B., Menviel, L., Leventer, A., Hope, J.M., Brocks, J.J., Fallon, S., Post, A.L., O'brien, P.E., Grant, K., Armand, L., 2023. Early sea ice decline off East Antarctica at the last glacial-interglacial climate transition. Sci. Adv. 9. https://doi.org/10.1126/sciadv.adh9513.
Scambos, T.A., Bohlander, J.A., Shuman, C.A., Skvarca, P., 2004. Glacier acceleration and thinning after ice shelf collapse in the Larsen B embayment, Antarctica. Geophys. Res. Lett. 31. https://doi.org/10.1029/2004GL020670.
Schlegel, N.J., Seroussi, H., Schodlok, M.P., Larour, E.Y., Boening, C., Limonadi, D., Watkins, M.M., Morlighem, M., Van Den Broeke, M.R., 2018. Exploration of Antarctic ice sheet 100-year contribution to sea level rise and associated model uncertainties using the ISSM framework. Cryosphere 12, 3511–3534. https://doi.org/10.5194/tc-12-3511-2018.
Schoof, C., 2007. Ice sheet grounding line dynamics: steady states, stability, and hysteresis. J. Geophys. Res. 112, 1–19. https://doi.org/10.1029/2006JF000664.
Schroeter, S., O'Kane, T.J., Sandery, P.A., 2023. Antarctic sea ice regime shift associated with decreasing zonal symmetry in the Southern Annular Mode. Cryosphere 17, 701–717. https://doi.org/10.5194/tc-17-701-2023.
Shakesby, R.A., Matthews, J.A., Owen, G., 2006. The schmidt hammer as a relative-age dating tool and its potential for calibrated-age dating in Holocene glaciated environments. Quat. Sci. Rev. 25, 2846–2867. https://doi.org/10.1016/j.quascirev.2006.07.011.
Small, D., Berg, S., White, D., 2025. Rapid relative sea-level fall, 8–6 ka, in the Windmill islands, East Antarctica. Quat. Sci. Rev. 365. https://doi.org/10.1016/j.quascirev.2025.109488.
Small, D., Fülöp, réka-H., Smedley, R., Lees, T., Trabucatti, S., Fabel, D., Miguens-Rodriguez, M., Smith, A., Boeckmann, G.. A thinner-than-present West Antarctic Ice Sheet in the southern Weddell Sea Embayment during the Holocene. *EGUsphere*, *[preprint]*. https://doi.org/10.5194/egusphere-2025-4794.
Souchez, R.A., 1967. The formation of shear moraines: an example from south Victoria land, Antarctica. J. Glaciol. 6, 837–843. https://doi.org/10.3189/s0022143000020141.
Stokes, C.R., Abram, N.J., Bentley, M.J., Edwards, T.L., England, M.H., Foppert, A., Jamieson, S.S.R., Jones, R.S., King, M.A., Lenaerts, J.T.M., Medley, B., Miles, B.W.J., Paxman, G.J.G., Ritz, C., van de Flierdt, T., Whitehouse, P.L., 2022. Response of the East Antarctic ice sheet to past and future climate change. Nature 608, 275–286. https://doi.org/10.1038/s41586-022-04946-0.
Suganuma, Y., Kaneda, H., Mas e Braga, M., Ishiwa, T., Koyama, T., Newall, J.C., Okuno, J., Obase, T., Saito, F., Rogozhina, I., Andersen, J.L., Kawamata, M., Hirabayashi, M., Lifton, N.A., Fredin, O., Harbor, J.M., Stroeven, A.P., Abe-Ouchi, A., 2022. Regional sea-level highstand triggered Holocene ice sheet thinning across coastal dronning maud land, East Antarctica. Commun. Earth Environ. 3. https://doi.org/10.1038/s43247-022-00599-z.
Thomas, R.H., Bentley, C.R., 1978. A model for Holocene retreat of the west antarctic Ice sheet. Quat Res 10, 150–170. https://doi.org/10.1016/0033-5894(78)90098-4.
Udy, D.G., Vance, T.R., Kiem, A.S., Holbrook, N.J., Curran, M.A.J., 2021. Links between large-scale modes of climate variability and synoptic weather patterns in the Southern Indian Ocean. J. Clim. 34, 883–899. https://doi.org/10.1175/JCLI-D-20.
Udy, D.G., Vance, T.R., Kiem, A.S., Holbrook, N.J., 2022. A synoptic bridge linking sea salt aerosol concentrations in East Antarctic snowfall to Australian rainfall. Commun. Earth Environ. 3. https://doi.org/10.1038/s43247-022-00502-w.
Van Ommen, T.D., Morgan, V., Curran, M.A.J., 2004. Deglacial and Holocene changes in accumulation at law dome, East Antarctica. Ann. Glaciol. 39, 359–365. https://doi.org/10.3189/172756404781814221.
Vance, T.R., Van Ommen, T.D., Curran, M.A.J., Plummer, C.T., Moy, A.D., 2013. A millennial proxy record of ENSO and eastern Australian rainfall from the law dome ice core, east Antarctica. J. Clim. 26, 710–725. https://doi.org/10.1175/JCLI-D-12-00003.1.
Verkulich, S.R., Melles, M., Hubberten, H.-W., 2002. Holocene environmental changes and development of figurnoye Lake in the southern Bunger hills, East Antarctica. J. Paleolimnol. 28, 253–267. https://doi.org/10.1023/A:1021661700899.
Verleyen, E., Tavernier, I., Hodgson, D.A., Whitehouse, P.L., Kudoh, S., Imura, S., Heirman, K., Bentley, M.J., Roberts, S.J., De Batist, M., Sabbe, K., Vyverman, W., 2017. Ice sheet retreat and glacio-isostatic adjustment in Lützow-holm Bay, East Antarctica. Quat. Sci. Rev. 169, 85–98. https://doi.org/10.1016/j.quascirev.2017.06.003.
Weertman, J., 1961. Mechanism for the formation of inner moraines found near the edge of cold ice caps and ice sheets. J. Glaciol. 3, 965–978. https://doi.org/10.3189/s0022143000017378.
White, D., 2021. Rock Weathering Observations of Surface Sediment in the Australian Antarctic Territory, Ver. 1. https://doi.org/10.26179/npxn-cz45.
White, D., 2024. Data from the Cosmogenic Nuclide Dating Program Following AAS 4318 'CADAGIA' Field Surveys, Ver.1. https://doi.org/10.26179/q9xm-ge23.
White, D.A., Fink, D., 2014. Late Quaternary glacial history constrains glacio-isostatic rebound in Enderby land, East Antarctica. J Geophys Res Earth Surf 119, 401–413. https://doi.org/10.1002/2013JF002870.
White, D.A., Bennike, O., Berg, S., Harley, S.L., Fink, D., Kiernan, K., McConnell, A., Wagner, B., 2009. Geomorphology and glacial history of Rauer group, East Antarctica. Quat Res 72, 80–90. https://doi.org/10.1016/j.yqres.2009.04.001.
White, D.A., Fink, D., Gore, D.B., 2011. Cosmogenic nuclide evidence for enhanced sensitivity of an East Antarctic ice stream to change during the last deglaciation. Geology 39 (1), 23–26. https://doi.org/10.1130/G31591.
White, D., Fink, D., Lilly, K., O'Brien, P., Dorschel, B., Berg, S., Bennike, O., Gore, D., Fabel, D., Blaxell, M., Jeromson, M., Codilean, A.T., Wilken, K.M., Galton-Fenzi, B., Wagner, B., 2022. Rapid ice sheet response to deglacial and Holocene paleoenvironmental changes in eastern Prydz Bay, East Antarctica. Quat. Sci. Rev. 280, 107401. https://doi.org/10.1016/J.QUASCIREV.2022.107401.
Whitehouse, P.L., Bentley, M.J., Milne, G.A., King, M.A., Thomas, I.D., 2012. A new glacial isostatic adjustment model for Antarctica: calibrated and tested using observations of relative sea-level change and present-day uplift rates. Geophys. J. Int. 190, 1464–1482. https://doi.org/10.1111/j.1365-246X.2012.05557.x.
Wilcken, K.M., Fink, D., Hotchkis, M.A.C., Garton, D., Button, D., Mann, M., Kitchen, R., Hauser, T., O'Connor, A., 2017. Accelerator mass spectrometry on SIRIUS: new 6 MV spectrometer at ANSTO. Nucl. Instrum. Methods Phys. Res. B 406, 278–282. https://doi.org/10.1016/j.nimb.2017.01.003.
Wilcken, K.M., Fujioka, T., Fink, D., Fülöp, R.H., Codilean, A.T., Simon, K., Mifsud, C., Kotevski, S., 2019. SIRIUS performance: 10Be, 26Al and 36Cl measurements at ANSTO. Nucl. Instrum. Methods Phys. Res. B 455, 300–304. https://doi.org/10.1016/j.nimb.2019.02.009.
Wilcken, K.M., Codilean, A.T., Fülöp, R.H., Kotevski, S., Rood, A.H., Rood, D.H., Seal, A. J., Simon, K., 2022. Technical note: accelerator mass spectrometry of 10Be and 26Al at low nuclide concentrations. Geochronology 4, 339–352. https://doi.org/10.5194/gchron-4-339-2022.
Wilson, D.J., Bertram, R.A., Needham, E.F., van de Flierdt, T., Welsh, K.J., McKay, R.M., Mazumder, A., Riesselman, C.R., Jimenez-Espejo, F.J., Escutia, C., 2018. Ice loss from the East Antarctic ice sheet during late Pleistocene interglacials. Nature 561, 383–386. https://doi.org/10.1038/s41586-018-0501-8.

Yamane, M., Yokoyama, Y., Miura, H., Maemoku, H., Iwasaki, S., Matsuzaki, H., 2011. The last deglacial history of Lützow-holm Bay, East Antarctica. J. Quat. Sci. 26, 3–6. https://doi.org/10.1002/jqs.1465.

Ye, W., Cheng, L., Kitade, Y., Hu, S., Zuo, J., 2024. Distribution of modified circumpolar deep water and its threat in Vincennes Bay, East Antarctica. J Oceanol Limnol 42, 1399–1414. https://doi.org/10.1007/s00343-024-3164-3.

Zhang, S.H., Zhao, Y., Liu, X.C., Liu, Y.S., Hou, K.J., Li, C.F., Ye, H., 2012. U-Pb geochronology and geochemistry of the bedrocks and moraine sediments from the Windmill islands: implications for Proterozoic evolution of East Antarctica. Precambr. Res. 206–207, 52–71. https://doi.org/10.1016/j.precamres.2012.02.019.

Zwally, H.J., Giovinetto, M.B., Beckley, M.A., Saba, J.L., 2012. Antarctic and Greenland Drainage Systems. GSFC Cryospheric Sciences Laboratory.